We are IntechOpen,
the world's leading publisher of
Open Access books
Built by scientists, for scientists

6,900
Open access books available

186,000
International authors and editors

200M
Downloads

154
Countries delivered to

Our authors are among the

TOP 1%
most cited scientists

12.2%
Contributors from top 500 universities

WEB OF SCIENCE™

Selection of our books indexed in the Book Citation Index
in Web of Science™ Core Collection (BKCI)

Interested in publishing with us?
Contact book.department@intechopen.com

Numbers displayed above are based on latest data collected.
For more information visit www.intechopen.com

The Development of Three-Intensity Measurement in PSA Ellipsometry and Photoelastic Modulation Ellipsometry

Yu-Faye Chao

Additional information is available at the end of the chapter

Abstract

A three-intensity measurement technique in a polarizer-sample-analyzer (PSA) ellipsometry will be introduced. The alignment of the azimuth angle of polarizer and analyzer to the incident plane will be discussed. Its applications to measure the ellipsometric parameters for deducing the optical parameters will be stated. In addition to the PSA ellipsometry, one can insert a photoelastic modulator (PEM) in the PSA ellipsometry for developing a PEM ellipsometry. There is no moving part in the system and its measuring speed is only limited by a modulator. An in situ/real-time and post-flight ellipsometry can be established for monitoring the dynamically varying process.

Keywords: alignment, calibrations, curved surface, real time

1. Introduction

The ellipsometry measures the change in polarization upon reflection or transmission [1] and then compares it with a model to deduce the optical parameters, such as the complex refractive index, film thickness, crystalline nature, and roughness of a sample. The ratio of the reflection coefficient in p-polarized light (r_p) to s-polarized light (r_s) has been noted as $\tan\Psi\, e^{i\Delta}$, where Ψ and Δ are the two ellipsometric parameters measured in ellipsometer. These parameters are very sensitive to the change in the optical response of incident radiation that interacts with the material. A commercial ellipsometer for measuring the thickness of a thin film has to achieve the precision within 2 Å in order to attract the IC industry for thin film measurement. This means the precision of Ψ and Δ have to be less than $0.02°$ and $0.04°$, respectively. In ellipsometry, the alignment and calibration are the crucial techniques for achieving these precisions. These techniques fully depend on the configuration of the system. First, one has to

establish the plane of incident by aligning the azimuth angle of polarizer and analyzer to the plane of incident, both of which are the fundamental components of ellipsometer. Collins [2] and Chao [3] applied the null technique and the intensity ratio technique to locate the azimuth zeros of polarizer (P) and analyzer (A) with respect to the plane of incident, respectively. Both methods are complicated and time consuming. Due to the development of symbolic computer program Mathematica, one can analytically obtain the zeros of polarizer and analyzer with respect to the incident plane. In this chapter, the azimuth zeros of P and A to the incident plane will be located by an intensity ratio method. By rotating the analyzer, a three-intensity mea-surement technique will be applied to measure the ellipsometric parameters. According to the theoretical models, one can deduce the optical parameters from the measured ellipsometric parameters. Since only three intensities are needed to be measured, the imaging ellipsometry can be established. By using the following models: (a) the film thickness of flat and curved surface; (b) the refractive indices of homogeneous and nonhomogeneous bulk medium; (c) focused beam for surface plasmon resonance (SPR) phenomena, one can prove that this simple imaging ellipsometry has many different applications.

The photoelastic modulator (PEM) will be introduced in the polarizer-sample-analyzer (PSA) ellipsometric system for an in situ/real-time ellipsometry. The in situ alignment technique of the optical axis of PEM is essential for establishing a real-time ellipsometry. Here, the real-time measurements of the ellipsometric parameters under etching and thermal heating processes will be presented. In addition to real time, one can also use the post-flight technique to analyze the digital waveform of an anisotropic medium.

2. The alignment in PSA ellipsometry

The PSA ellipsometry setup is shown in **Figure 1**. Before inserting the PEM, one can setup the PSA ellipsometry for three-intensity measurement. For aligning the azimuth angles of P and A with respect to the incident plane, one can setup the PSA configuration in the interested incident angle (typical 70° in IC industry). The measured reflected intensity is expressed in the ellipsometric parameters, Ψ, Δ, and azimuth angles of P and A:

$$I(P, A) = I_0 \left[\sin^2 P \, \sin^2 A + \tan^2 \Psi \, \cos^2 P \, \cos^2 A + \frac{1}{2} \tan \Psi \, \cos \Delta \, \sin 2P \, \sin 2A \right] \quad (1)$$

By considering the polarizer and analyzer separately, Chao [4] improved Steel's [5] intensity ratio technique to align the polarizer and analyzer to the incident plane. For alignment, the following intensity ratios A and B are defined:

$$A(\alpha, \beta) = \frac{I(45° + \alpha, \beta)}{I(45° + \alpha, 90° + \beta)} \quad (2)$$

$$B(\alpha, \beta) = \frac{I(-45° + \alpha, \beta)}{I(-45° + \alpha, 90° + \beta)} \quad (3)$$
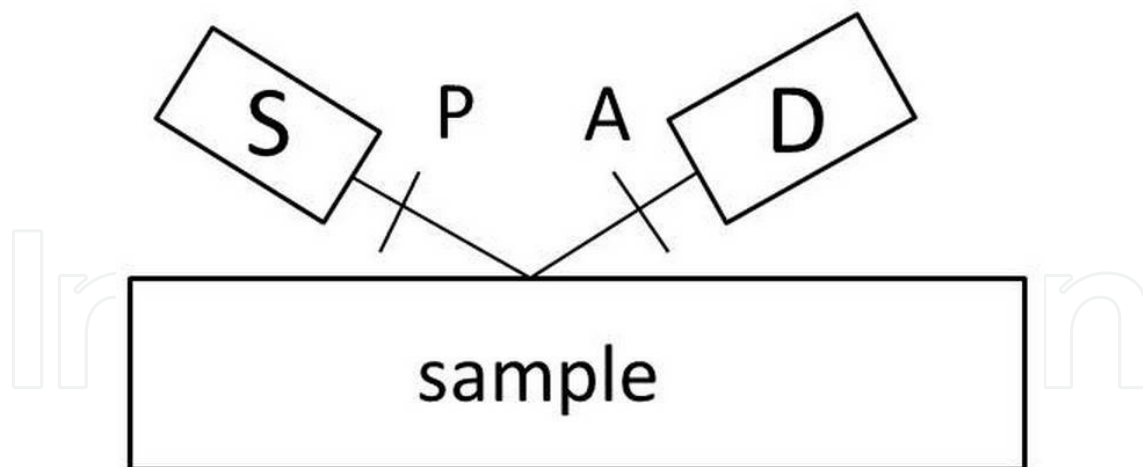
Figure 1. Schematic setup of PSA ellipsometry: A: analyzer, S, light source; P, polarizer; D, detector.

In addition to the azimuth angle of P and A, the small angle deviation α and β from the incident plane, respectively, are considered. These intensity ratios are expanded to the first-order approximation around their respective scales, and expressed as follows:

$$A(\alpha, \beta) \cong \tan^2 \psi - 2\left[2\tan^2 \Psi \ \alpha - \sec^2 \Psi \ \tan \Psi \ \cos \Delta \ \beta\right] \tag{4}$$

$$B(\alpha, \beta) \cong \tan^2 \Psi + 2\left[2\tan^2 \Psi \ \alpha - \sec^2 \Psi \ \tan \Psi \ \cos \Delta \ \beta\right] \tag{5}$$

These two equations intersect with each other when

$$2\tan^2 \Psi \ \alpha - \sec^2 \Psi \ \tan \Psi \ \cos \Delta \ \beta = 0 \tag{6}$$

so the deviation of α and β can be easily obtained for the opposite of $\cos\Delta$. Two incident angles [3], and fixed incident angle by two samples and two wavelengths [6] are proposed to align the azimuth angles of polarizer and analyzer. These complicated processes can be substituted by an analytical measurement technique [7]. In polar coordinates, if the incident light is $E_p = E_s$, the reflected intensity is distributed in an elliptical form [5] as shown in **Figure 2**, which can be formulated as

$$I(A) = L\cos^2(A - \theta) + T\sin^2(A - \theta) \tag{7}$$

where L and T are the magnitudes of the maximum and minimum intensities, respectively, and θ is the azimuth of maximum intensity. Since there are only three unknowns, one can measure three intensities to deduce the three parameters. Eq. (7) can also be written as follows:

$$I(A) = B(1 + C\cos 2A + D\sin 2A) \tag{8}$$

where the parameters B, C, and D can be written in terms of L, T, and θ, that is, B = 0.5(L+T), C = (L−T)cos2θ/(L+T), and D = (L−T)sin2θ/(L+T). It is easy to prove that parameters B, C, and D can be measured by three intensities measured at A = 0°, 60°, and 120°;

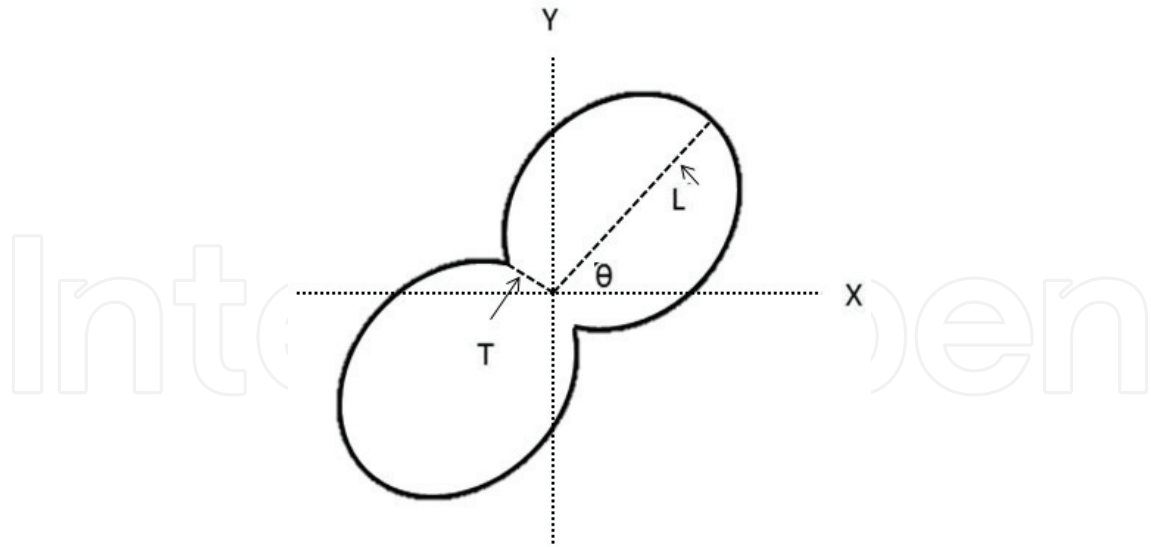**Figure 2.** Intensity distribution in polar coordinates at various azimuth angles of analyzer.

$$B = \frac{1}{3}[I(0°) + I(60°) + I(120°)] \tag{9}$$

$$C = 2 - [I(60°) + I(120°)]/B \tag{10}$$

$$D = \frac{1}{B\sqrt{3}}[I(60°) - I(120°)] \tag{11}$$

So, $\tan 2\theta = D/C$; $L = B + DB/\sin 2\theta$ and $T = 2B - L$. By comparing the expansion of Eq. (1), one can obtain the following relationships:

$$\tan 2\theta = \frac{\cos\Delta \; \sin 2P \; \sin 2\Psi}{\cos 2P - \cos 2\Psi} \tag{12}$$

$$\tan^2\Psi = \frac{1 + C}{1 - C}\tan^2 P \tag{13}$$

$$\frac{(L - T)^2}{4LT}\sin^2 2\theta = \cot^2\Delta \tag{14}$$

when there is no deviation in the azimuth angles of polarizer and analyzer. Even there are deviations α and β for P and A, respectively, one can substitute those errors in the previous relations and obtain the analytical results, that is

$$\sin 2\alpha = \frac{1 - \sqrt{\frac{(1+C_1)(1-C_2)}{(1-C_1)(1+C_2)}}}{1 + \sqrt{\frac{(1+C_1)(1-C_2)}{(1-C_1)(1+C_2)}}} \tag{15}$$

$$\tan\Psi = 4\sqrt{\frac{1 - \sqrt{\frac{(1+C_1)(1-C_2)}{(1-C_1)(1+C_2)}}}{1 + \sqrt{\frac{(1+C_1)(1-C_2)}{(1-C_1)(1+C_2)}}}} \tag{16}$$

$$\beta = \frac{1}{4}\left(\tan^{-1}\frac{D_1}{C_1} - \tan^{-1}\frac{D_2}{C_2} \right) \tag{17}$$

where subscripts 1 and 2 indicate the three-intensity measurement obtained at P = 45° and −45°, respectively. After correction, the value Δ can be obtained by substituting the corrected value into the appropriate relation. The most important aspect of this technique is the concept of direct determination, in contrast to locating the minimum intensity in the null ellipsometry, which not only requires a sensitivity detector but also requires a polarizer with a high extinction ratio. This intensity ratio technique only needs a minimum amount of data to deduce the deviations and ellipsometric parameters simultaneously. If the detector is a high-dynamic range detector, the precision of this three-intensity measurement technique will be compatible to the commercial ellipsometer. Moreover, a complicated alignment process is not required in the simple PSA ellipsometry.

3. Three-intensity measurements technique in PSA ellipsometry

The analytical alignment technique provides a simple and accurate alignment technique in ellipsometry. Since only three-intensity measurements are required, one can use charge-coupled device (CCD) as a detector for imaging ellipsometry.

3.1. Film thickness of SiO$_2$/Si thin film

In the beginning, the azimuth angles of polarizer and analyzer are aligned to the incident plane by the Brewster angle of a nonabsorbent as the reference zero. After the rough alignment, the azimuth angle of polarizer is set at 45° and −45°, respectively, for analyzer to be at three angles, that is, 0°, 60°, and 120°, and the corresponding three-intensity measurements. One can choose an appropriate incident angle (typical 70°) for ellipsometric measurements. Using the relations in the last section, one can calculate Ψ, Δ, α, and β from three-intensity measurements. According to the definition of ellipsometric parameters to Fresnel reflection coefficient [1], one can deduce the film thickness of thin film (SiO$_2$/Si thin film) through computer program. The primary objective is to compare the ellipsometric parameters measured with rough alignment to the analytically corrected values. Just as expected, the system errors are clearly observable in the deduced values of Ψ and Δ, measured at P = 45° and −45° separately, as shown in **Figure 3**. After readjusting the azimuth angles of polarizer and analyzer, one can observe the flat distribution of Ψ and Δ measured at P = 45° and −45°. The corrected ellipsometric parameters of the results deviated from each other by less than 0.01°, as shown in **Tables 1** and **2**. The corrected values are used for film thickness deduction. It is known that a rotating polarizer ellipsometry can deviate the incident angle [8]; the incident angle for thickness deduction is 69.94° instead of 70°.

3.2. Imaging ellipsometry

In the PSA ellipsometry, one can add a beam expander and use CCD as a detector, such as shown in **Figure 4**. This imaging ellipsometry can measure the refractive index of a flat bulk
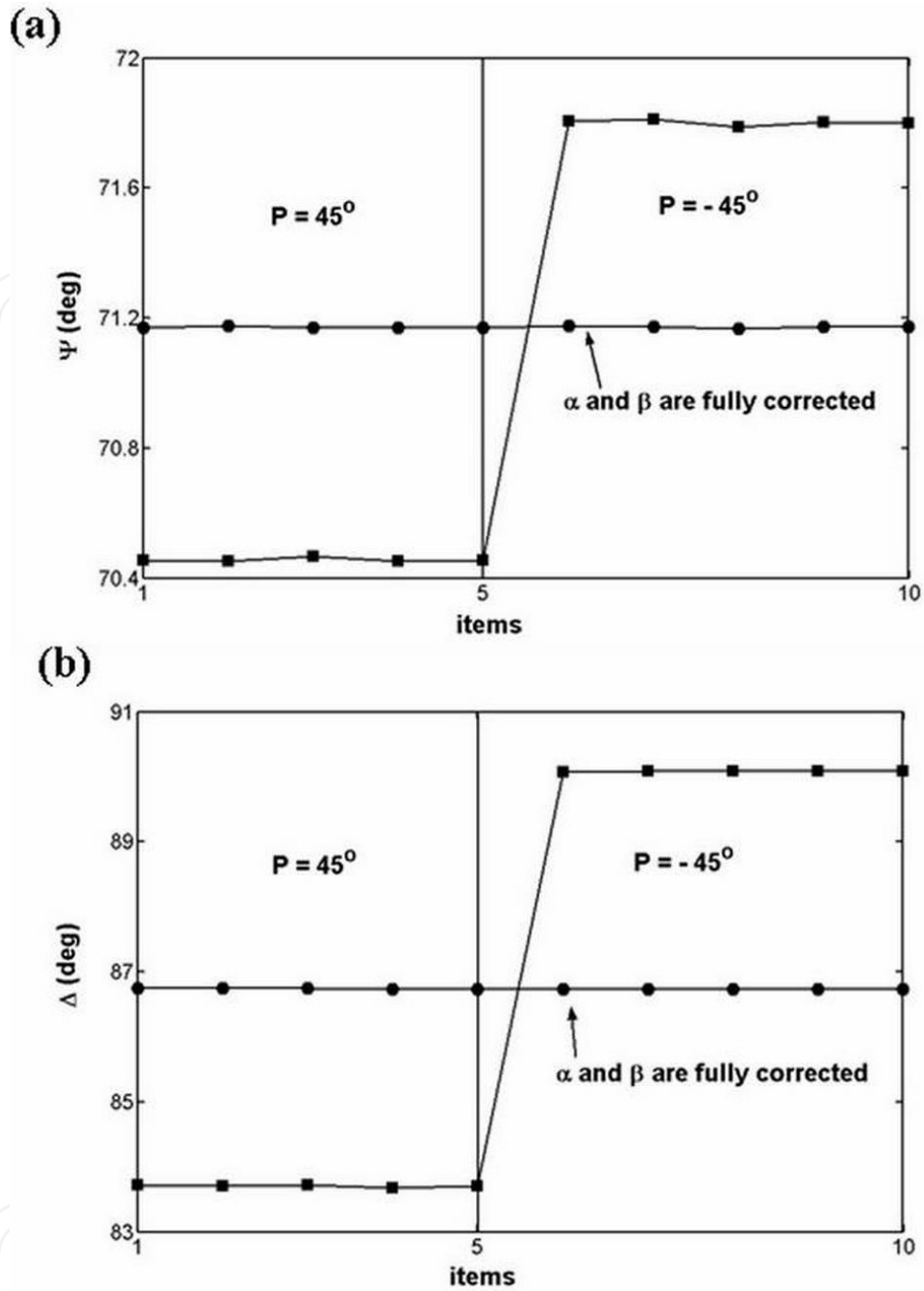
Figure 3. Ellipsometric measurements of PSA ellipsometry for a SiO$_2$ film on a Si substrate: (a) ψ and (b) Δ measured after a rough alignment (filled squares) at P = 45°and −45°, where α = 0.998±0.011° and β = 1.233±0.005° and after readjusted (filled circles) at P = 45° and −45°, where α = 0.015±0.009° and β = 0.006±0.003°.

medium, curved surface, and film thickness on a curved surface. Moreover, the SPR phenomena will be presented by a focused light beam.

3.2.1. Refractive index of flat surface of a bulk medium

Since there is no multiple reflection on a bulk medium, the refractive index of a bulk medium can be easily obtained by the ellipsometric parameter from the following relationship, let ρ = tanΨ e$^{i\Delta}$, then

Experiment	'ψ (deg)	Δ (deg)	Thickness (nm)	α (deg)	β (deg)
1	71.172	86.742	129.89	0.993	−1.229
2	71.175	86.745	129.93	1.000	−1.234
3	71.169	86.754	129.85	0.968	−1.231
4	71.171	86.727	129.88	0.991	−1.241
Mean	71.171	86.741	129.88	0.988	−1.233
Standard deviation	0.003	0.011	0.03	0.011	0.005
Jobin-Yvon ellipsometer			129.3		

Table 1. Optimized ellipsometric measurements of PSA ellipsometry for a SiO_2 film on a Si substrate after rough alignment.

Experiment	'ψ (deg)	Δ (deg)	Thickness (nm)	α (deg)	β (deg)
1	71.176	86.739	129.94	0.017	−0.011
2	71.174	86.731	129.93	0.013	−0.005
3	71.166	86.728	129.87	0.003	−0.005
4	71.174	86.726	129.91	0.026	−0.004
Mean	71.173	86.731	129.91	0.015	−0.006
Standard deviation	0.004	0.006	0.03	0.009	0.003

Table 2. Optimized ellipsometric measurements of PSA ellipsometry for a SiO_2 film on a Si substrate after readjusting azimuth angles of polarizer and analyzer.
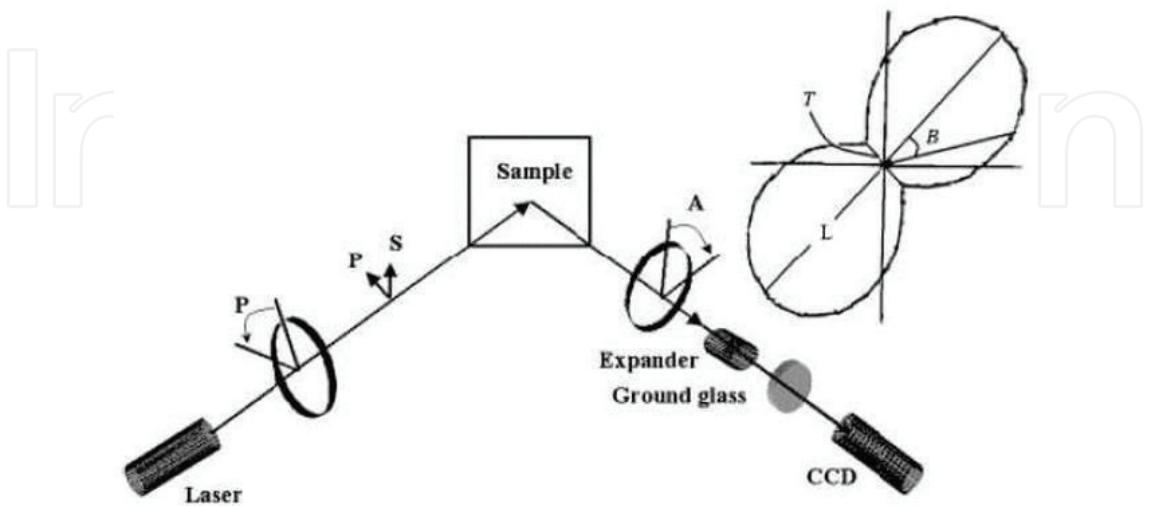

Figure 4. Schematic setup of the PSA imaging ellipsometer: Laser; P, polarizer; A, analyzer; S, sample; Expander, beam expander, and CCD camera. The elliptically distributed intensity on the right is under various azimuth angles of A in the polar coordinates.

$$n_1 = n_0 \tan \theta_i \left[1 - \frac{4\rho}{(1+\rho)^2} \sin^2 \theta_i \right]^{\frac{1}{2}} \tag{18}$$

where n_1, n_0 are the refractive indices of bulk medium and incident medium, respectively. θ_i is the incident angle.

The graded index structure has been widely used in fiber communication, in technologies such as the graded index fiber, and the gradient-index (GRIN) lens. The knowledge of the refractive index profile (RIP) of this graded index structure is important not only to assess its performance in optical devices but also to control the quality of products [9]. Since it is very important to measure the RIP of a gradient index material, the nondestructive measurement using imaging ellipsometry is suggested. The well-known material BK7 glass can be used to evaluate this imaging ellipsometry, such as shown in **Figure 5**. Since glass is nonabsorbent, the refractive index can be obtained by Ψ. In addition, the RIP of a gradient index fiber can be measured; its surface property can also be examined by α, such as shown in **Figure 6**, which will be proved that it is the direction of surface's normal.

3.2.2. The curved surface

Surface topography is a topic of great interest to science, technology, and industry. Both the contact stylus-based instruments [10] and noncontact optical instruments [11] can be used to measure and characterize the topography of a surface. By performing the ellipsometric measurements at two azimuth angles of the polarizer that differ by 90°, one can determine the azimuth deviation (α) of polarizer with respect to the incident plan by the three-intensity technique of PSA ellipsometry. After adjusting the deviation, one can prove that the azimuth
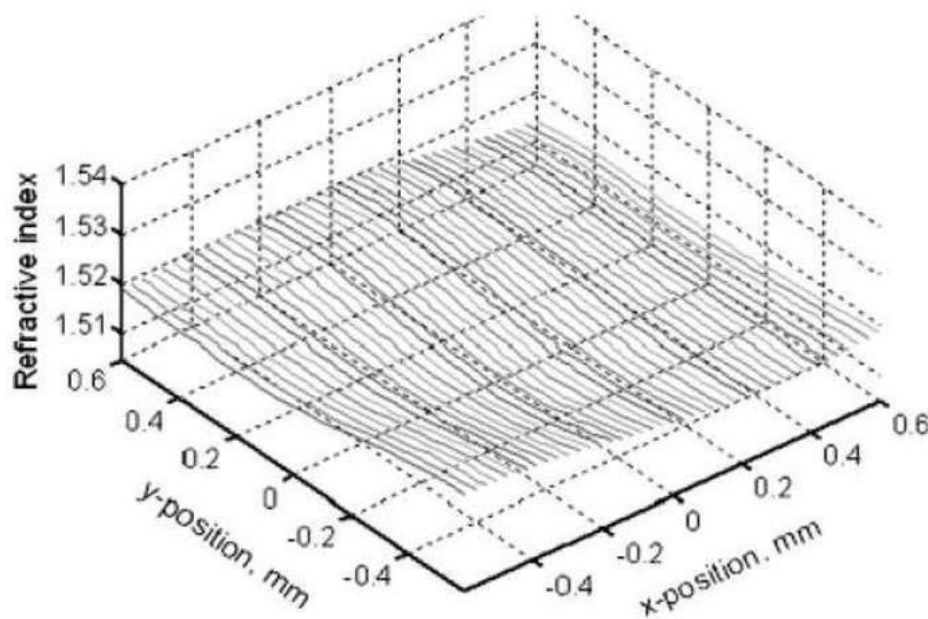

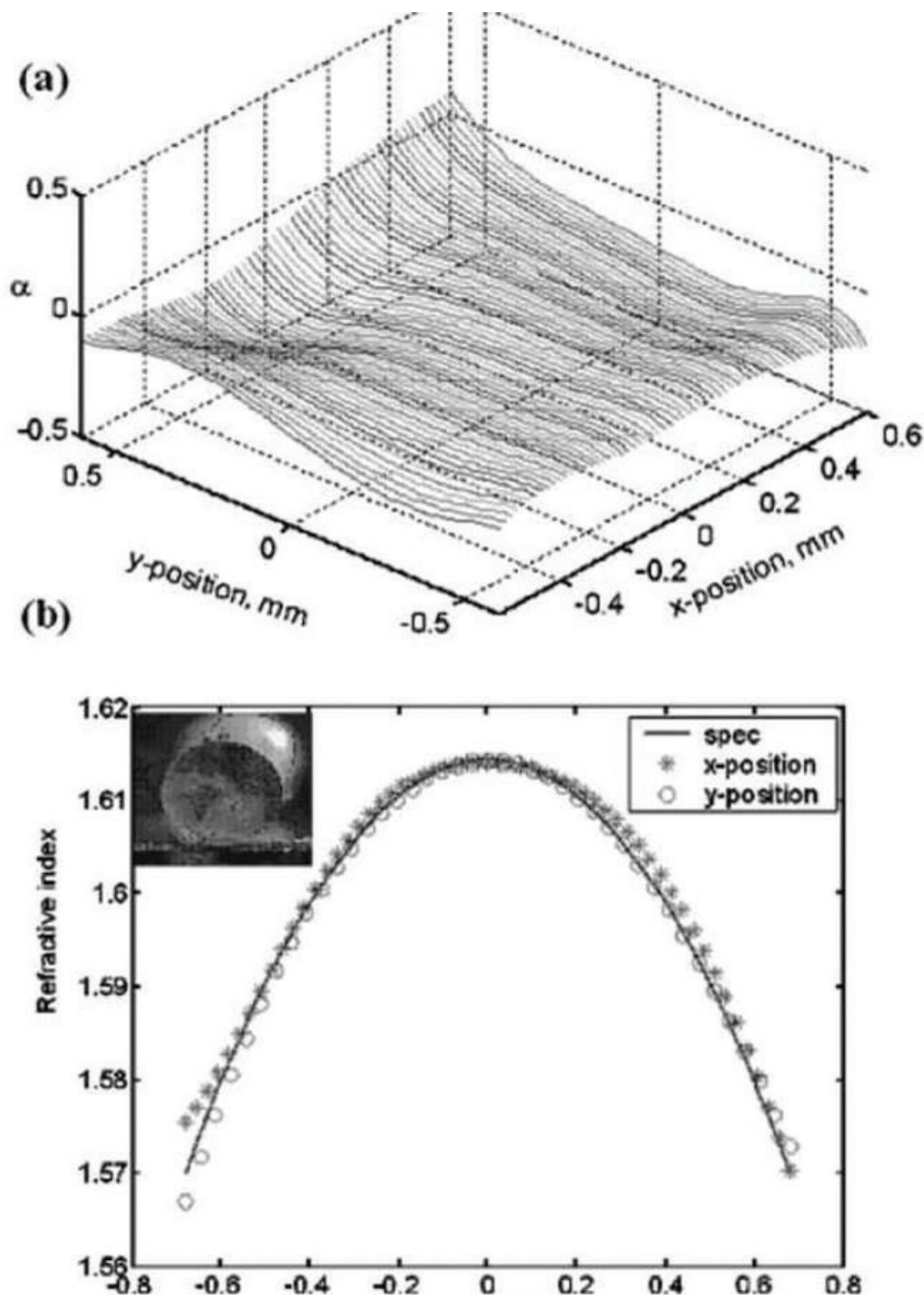**Figure 5.** Imaging ellipsometric study of a BK7 glass: n = 1.520±0.003.

Figure 6. Imaging ellipsometric study of a flat GRIN lens: (a) azimuth deviation (α) of the surface. (b) Measured refractive index profile (*: x-axis, ○: y-axis, solid line: RIP provided by NSG).

deviation of polarizer measured by this imaging ellipsometry can be used to measure the surface's normal; thus, it can be used to measure the surface topography of a lens. In the beginning, the alcohol surface is regarded as a flat surface for calibration; then one can tilt an SiO_2/Si sample for investigating its effect to the azimuth deviation of polarizer. In the previous section, the refractive index profile of a GRIN lens has been obtained. Here, one can use the same technique to measure the RIP of the diluted alcohol, such as shown in **Figure 7**. Since both the GRIN lens and diluted alcohol have flat surfaces, their azimuth deviations are near to zero. Tilting a plate confirms that α can be used to measure the normal line of the surface, such as shown in **Figure 8**. After understanding the meaning of α, one can measure the refractive index of a BK7 plano-convex lens and its surface's normal, such as shown in **Figure 9**. This can be flattened by correcting the α, as shown in **Figure 10**. Furthermore, one can rotate the tilted SiO_2/Si to investigate the three-direction cosines of the surface's normal. From the top view of a tilted plane, such as shown in **Figure 11b**, one can identify the surface's normal deviated by the tilted angle Θ with components α, and $\Delta\theta$ along x- and y-axes, respectively. The measured deviation α is the surface's normal projected on x-axis, which is perpendicular to the intersection of incident plane and sample surface. $\Delta\theta$ is the deviation of the incident angle caused by the tilting and can be deduced from the three-direction cosines. Three positions are examined, **Table 3**; all these results can be used to deduce the thickness of the thin film SiO_2 on silicon substrate [12]. For simplicity, one shall use a cylindrical lens and set it up as in **Figure 12**, then examine the thickness of its coating by the three-intensity measurements technique, the
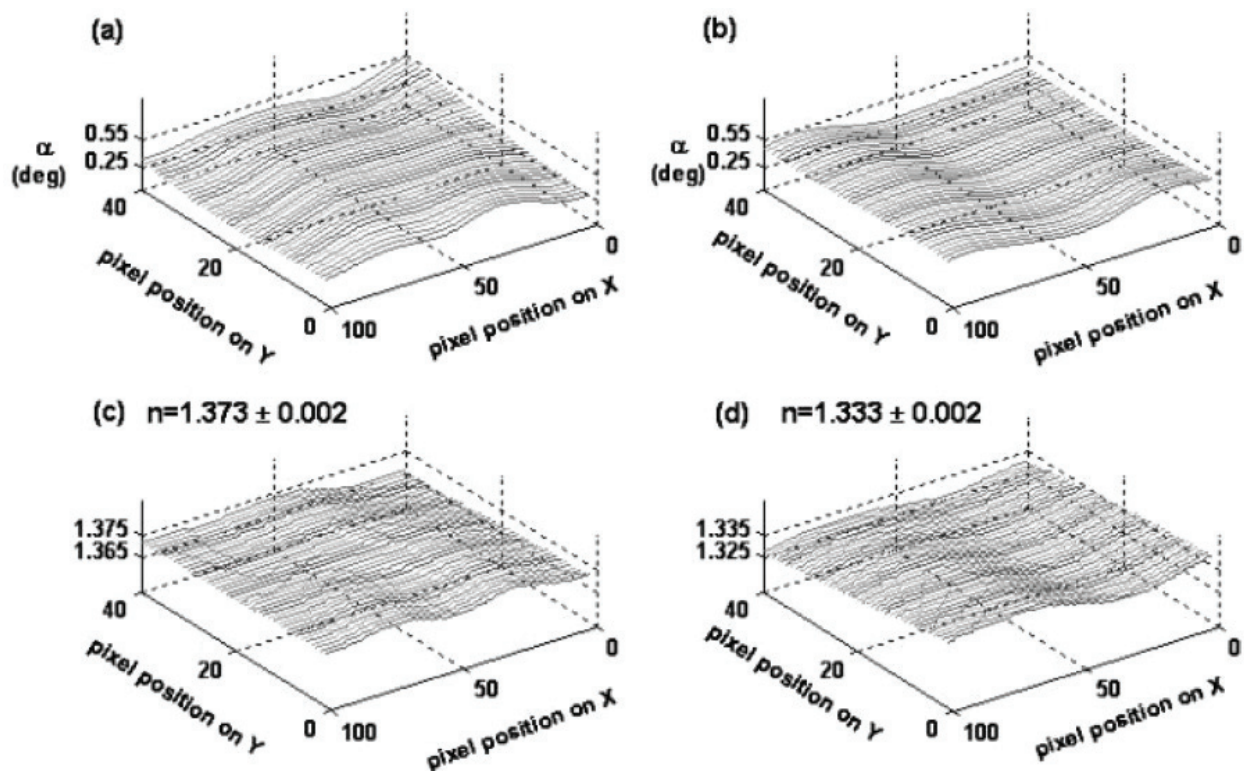

Figure 7. Imaging ellipsometric study of water and diluted alcohol: (a) azimuth deviation (α) of the diluted alcohol surface, (b) azimuth deviation (α) of the water surface, (c) refractive index profile of diluted alcohol n = 1.373 $\pm$ 0.002, and (d) refractive index profile of water n = 1.333 $\pm$ 0.002.
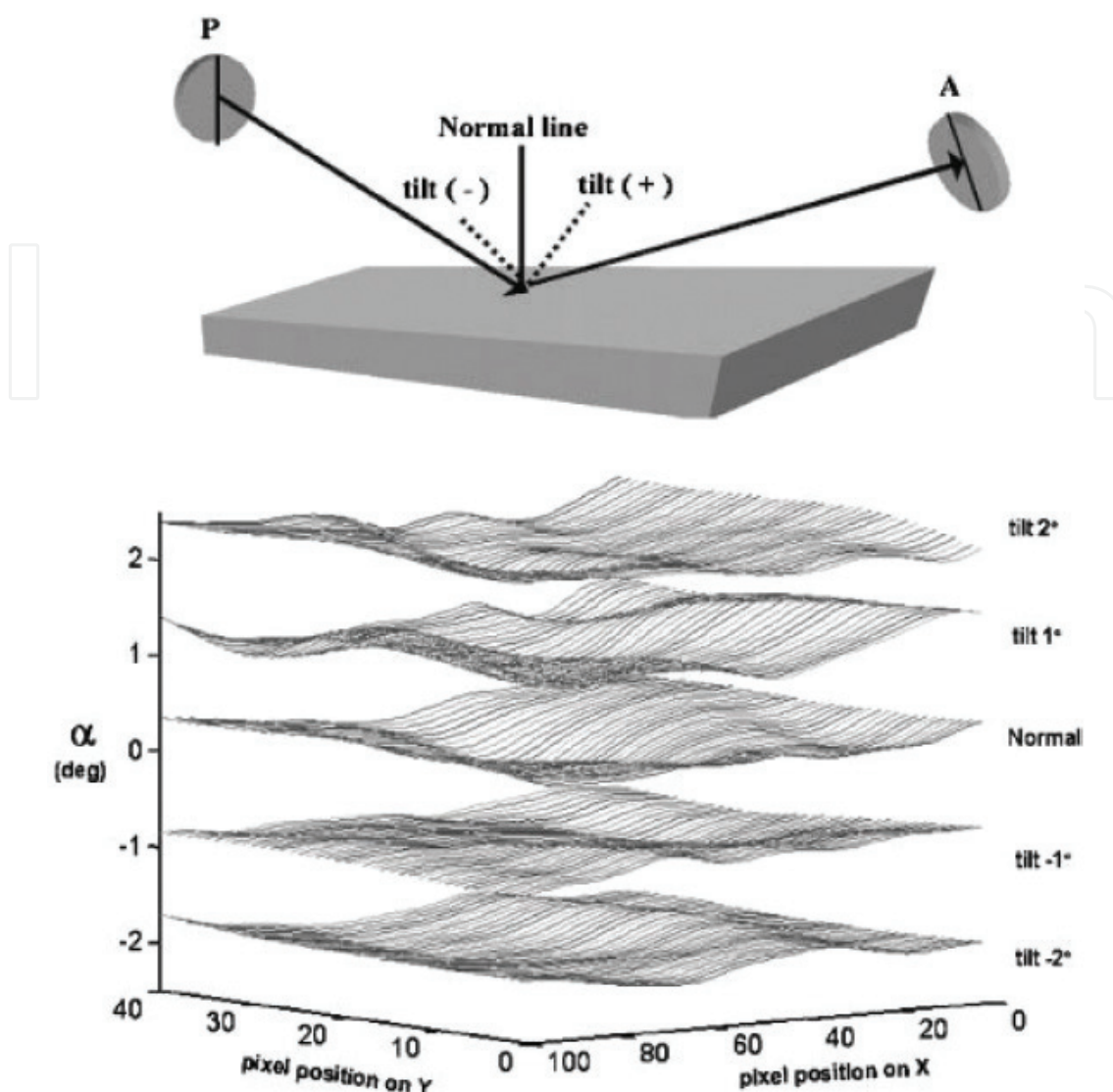
Figure 8. Imaging ellipsometric study of azimuth deviation of polarizer (a) caused by the tilting of a SiO$_2$ thin film on Si substrate. The thin film is tilted from −2 to 2° with step 1°.

measured Ψ and Δ are shown in **Figure 13**. In this configuration, the measured α is zero at the vertex of the cylinder. The corrected Ψ and Δ are flat which can be used to deduct the thickness of the coating. In conclusion, this three-intensity measurement technique can perform a measurement on thin film coating of a curved and titled surface with high precision.

3.2.3. Focused beam and surface plasmon resonance

In conventional ellipsometry, the light beam has to be collimated carefully to avoid the polarization errors. In the last section, we show that one can perform the ellipsometric measurement of a curved surface. Since the three-direction cosines have been well understood, one can measure a convergent/ divergent beam without any restriction [13]. Using a focused beam in the PSA imaging ellipsometry, one can perform the ellipsometric measurement under the surface plasmon resonance (SPR) condition and observe the resonance phenomena.
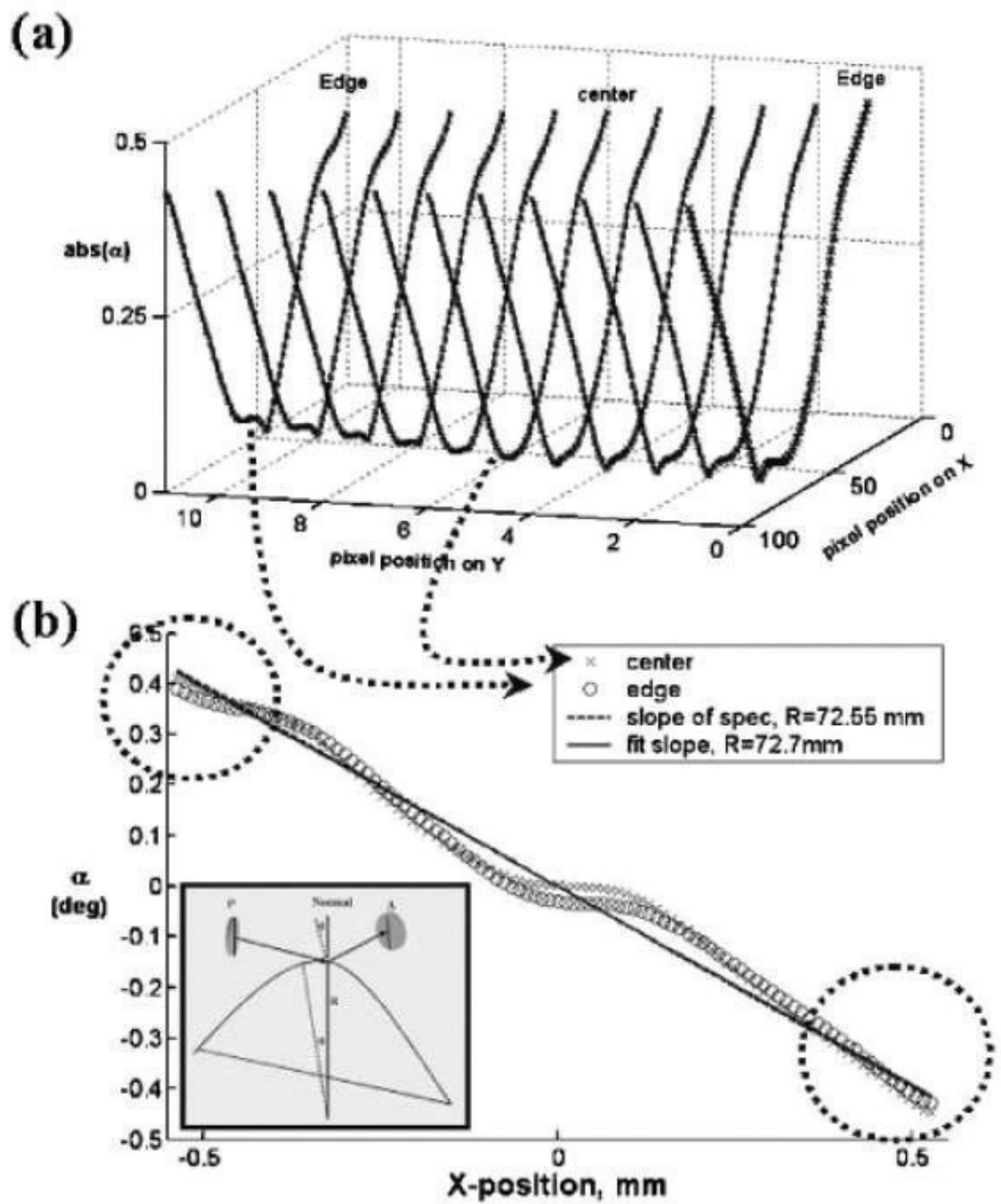
Figure 9. Imaging ellipsometric study of the radius of curvature of the BK7 plano-convex lens: (a) the magnitude of the azimuth deviation (α) of the surface and (b) the derived and measured α of the lens at the center and the edge (dashed line: derived from the radius measured by the Zygo phase-shift interferometer, solid line: measured by the imaging ellipsometric technique).
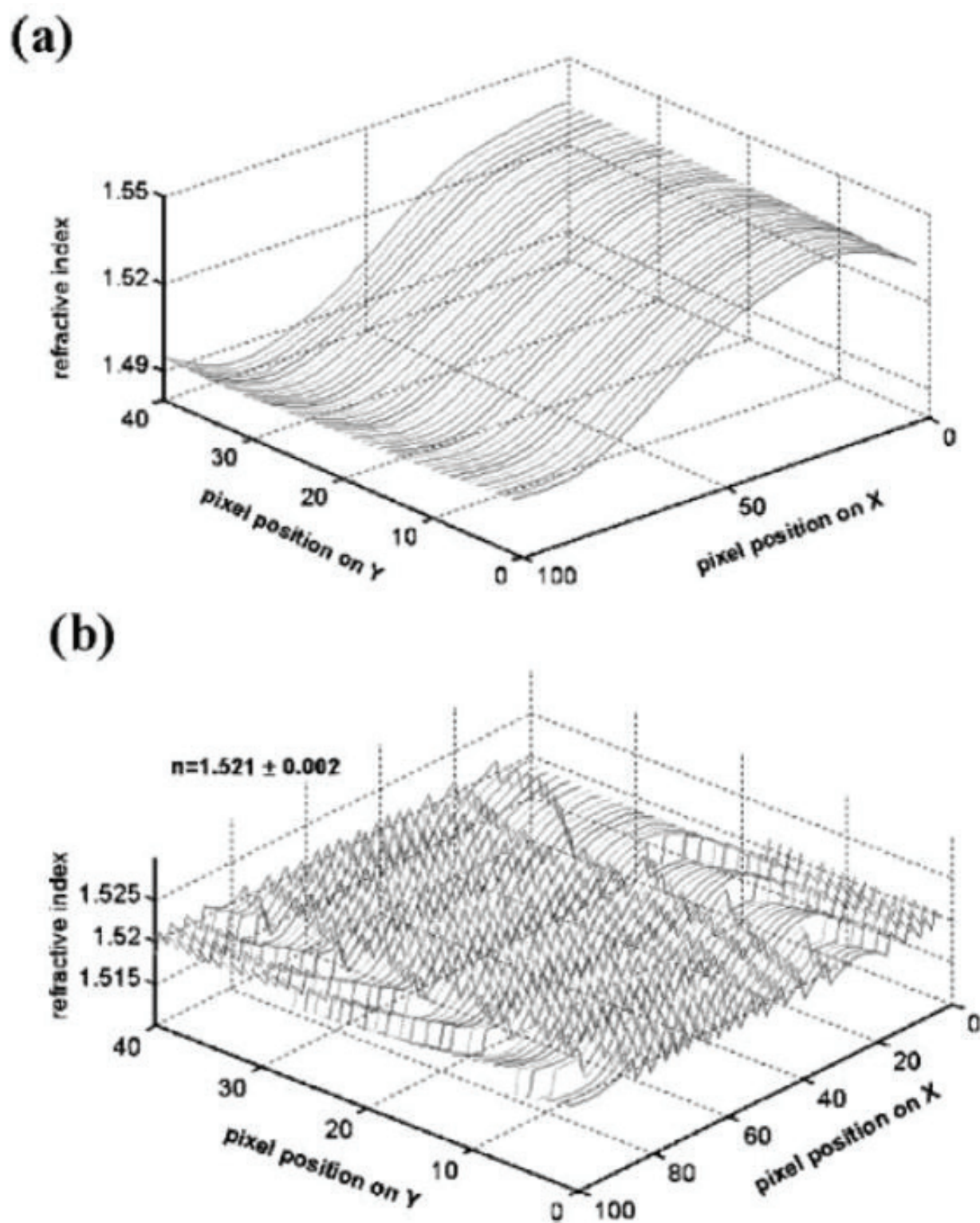
Figure 10. Imaging ellipsometric study of the RIP of the BK7 plano-convex lens: (a) the deduced RIP by considering the incident angle at 70° and (b) the deduced RIP by substituting its corresponding incident angles.
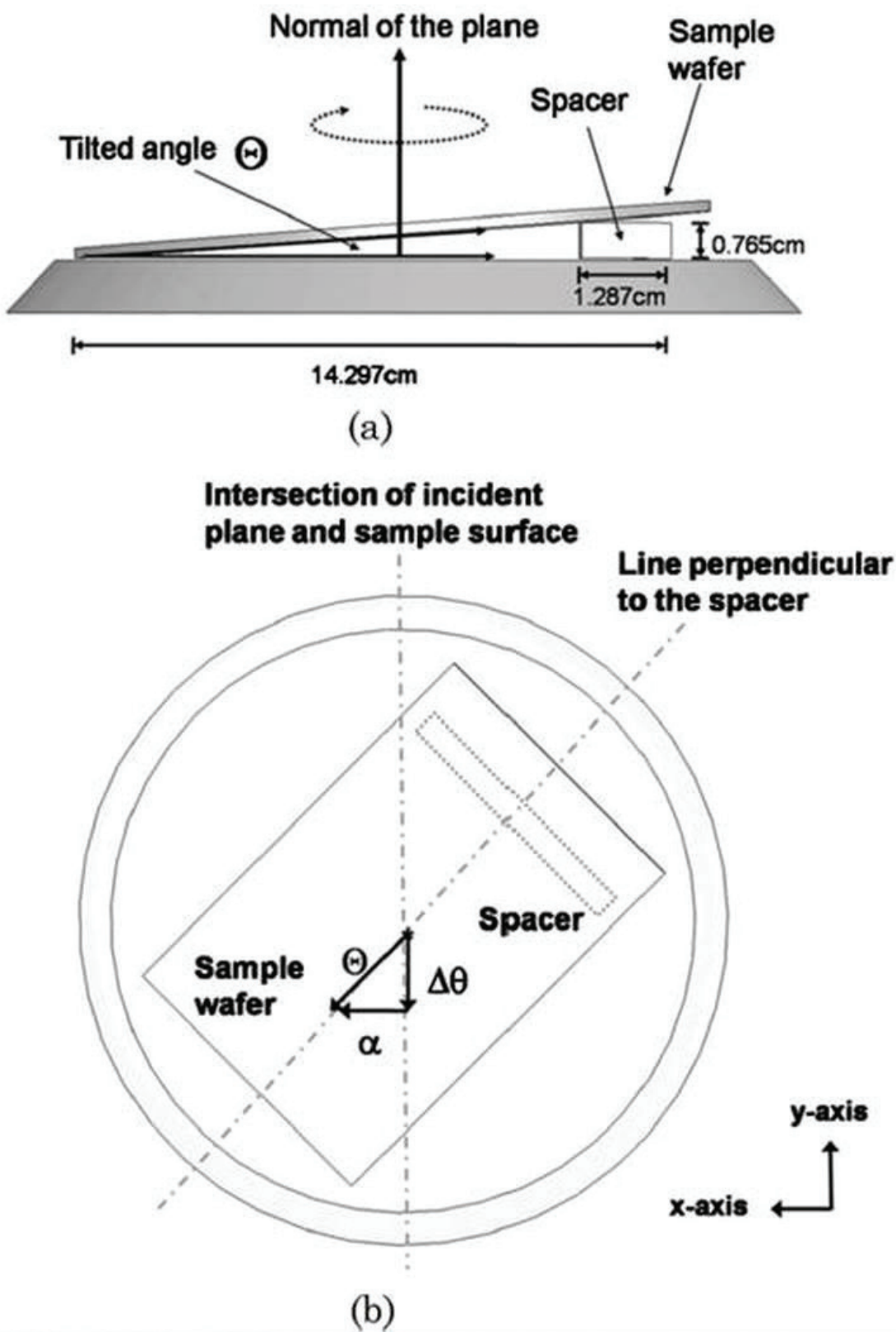
Figure 11. Schematic configuration of a tilted sample: (a) side view and (b) top view that indicates the motion of its surface normal: Θ, the tilted angle by spacer; $\Delta\theta$, the component that contributes to the incident angle variation; α, the component measured in the deviation of the polarizer.

Condition	Ψ (deg)	Δ (deg)	α (deg)	Δα (deg)	θ[a] (deg)	Δθ (deg)	Θ[a] (deg)
Untilted	69.28	90.35	0.02	2.59	69.76	1.35	2.94
Tilted	69.68	99.42	−2:57		68.41		
Untilted	69.08	90.40	0.06	2.75	69.73	1.06	2.94
Tilted	66.69	97.71	−2:69		68.67		
Untilted	69.24	90.42	0.06	2.95	69.75	0.08	2.94
Tilted	68.89	89.71	−2:89		69.83		

[a]θ, the incident angle; Θ, the tilted angle; the relationship of the three-direction cosine is $\cos^2\Theta = 1 - [\sin^2\Delta\alpha + \sin^2\Delta\theta]$.

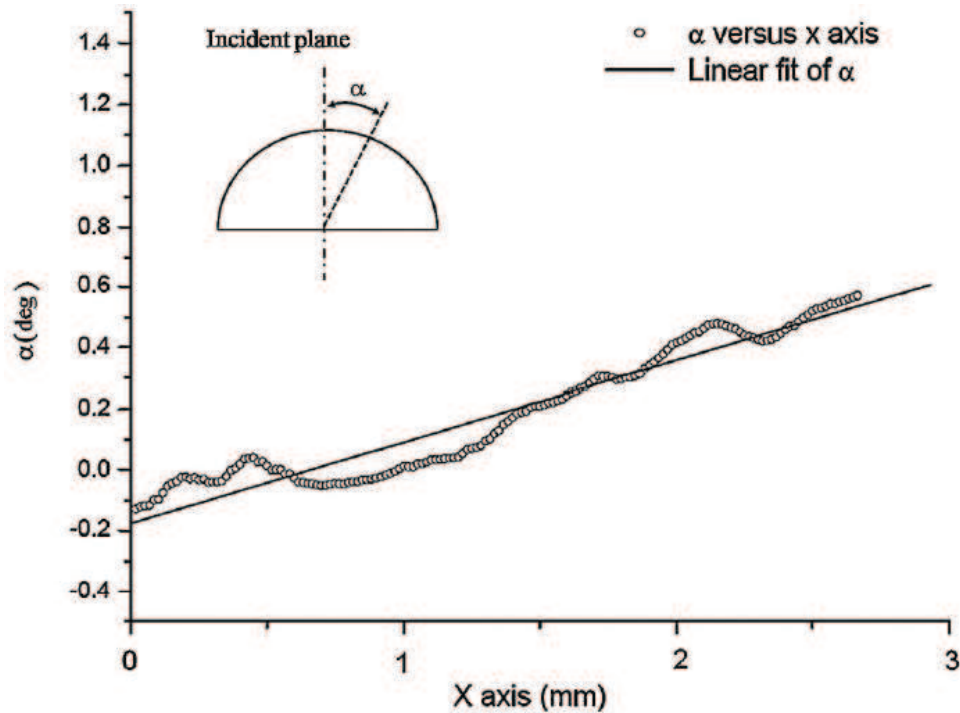**Table 3.** Ellipsometric measurements of tilted and untilted samples.

Figure 12. Deviation angle of the surface normal across the vertex of a cylindrical lens: open circles, measured α across the vertex of the lens; solid line, its best linear fit.

A cylindrical lens is used to produce a fan-shaped beam for multiple incident angles configuration. This can simplify the analysis to be a two-dimensional case. The three-intensity measurement technique can measure the ellipsometric parameters against each incidence angle but do not have to calibrate the azimuth errors of polarizer and analyzer. As a result of multiple incident angles approach, the whole Ψ curve around the SPR region can be obtained without rotating the sensor chip. The basic setup of the SPR sensor chip is in Kretchmann's configuration, such as shown in **Figure 14**. The beam can be expanded by a beam expander, then focused it on the base of a prism/biosensor around the resonance incident angle (air: 44°). One can measure the three intensities when P is at 45° and −45°, respectively. The measured intensities
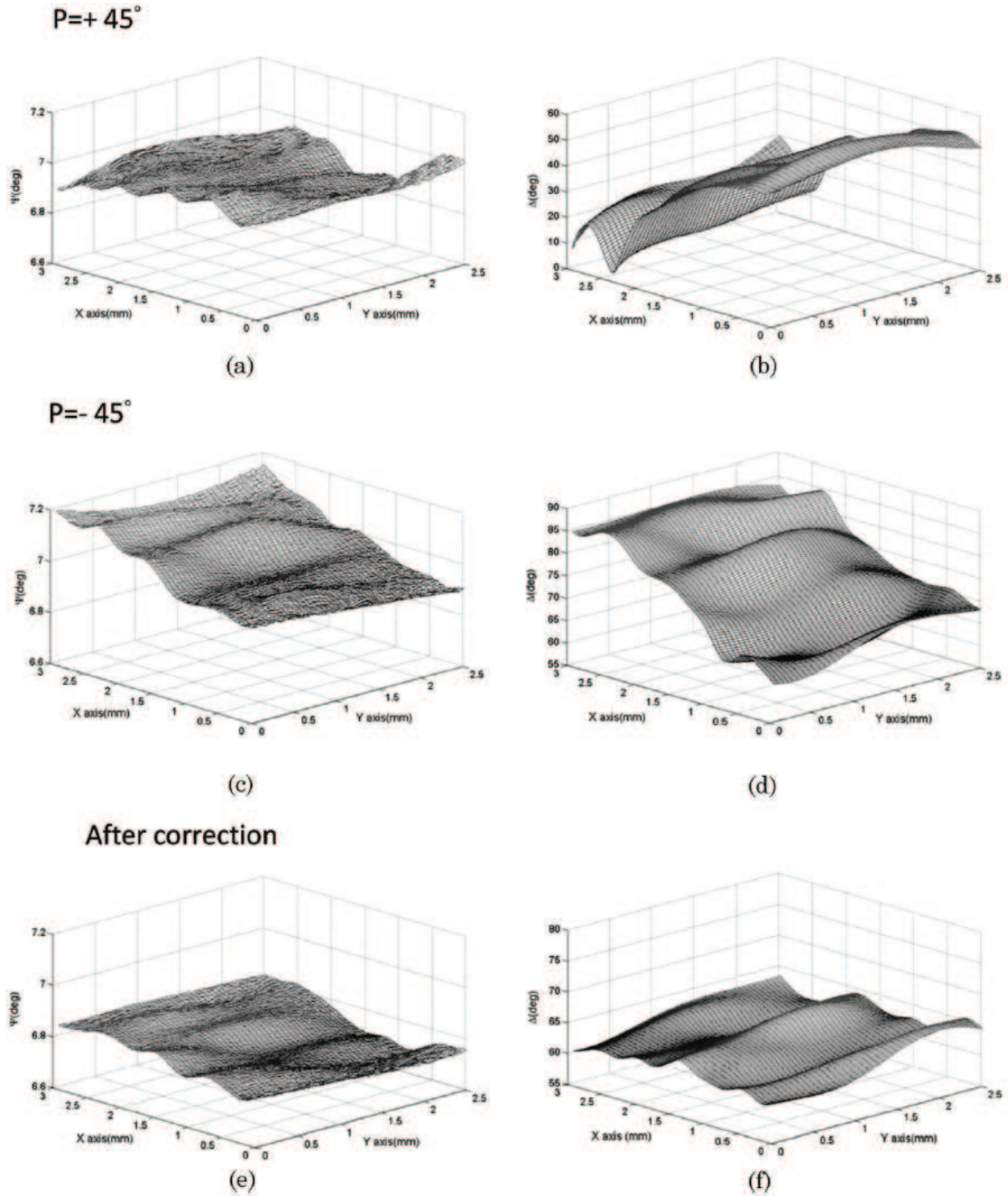
P=+ 45°

(a)

(b)

P=- 45°

(c)

(d)

After correction

(e)

(f)

Figure 13. Ellipsometric parameters and thickness profile of the cylindrical lens: (a) Ψ and (b) Δ measured when P = 45°; (c) Ψ and (d) Δ measured when P = −45°; (e) Ψ and (f) Δ after correction. Film thickness is 100±4.3 nm.

can be converted into ellipsometric parameters Ψ and Δ. Since the SPR phenomenon is more clearly observable by Ψ, we would like to present it by the distribution of Ψ versus the incident angle. The sensor chip is in Au/air (**Figure 15**) assembly. The solid line in the figure represents the theoretical value. This result can be used for calibration before other measurements.
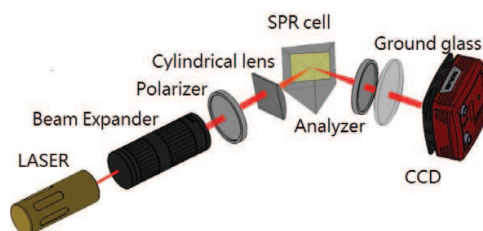
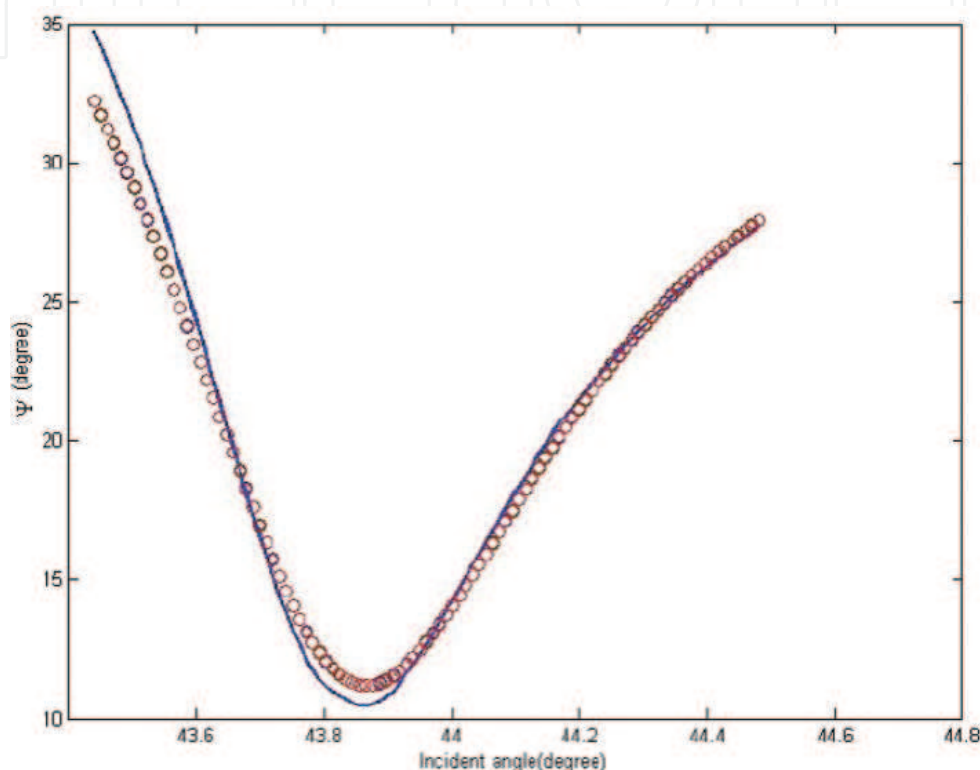**Figure 14.** The schematic setup of SPR for imaging ellipsometry.

Figure 15. The distribution of Ψ versus incident angle of the sensor chip in air (circles are the measured value; solid line is the theoretical value).

4. PEM ellipsometry

In PSA ellipsometry, one has to rotate both polarizer and analyzer in order to measure the ellipsometric parameters. These rotations do cause the incident angle to deviate from the setup and slow down the speed of measurements. In the beginning of 1990, the real-time/in situ ellipsometric system has started to develop. By inserting a PEM in the PSA ellipsometry, one can construct an ellipsometry without any mechanical motion and thus substantially increase the speed of measurement. A photoelastic modulator (PEM) is a device that utilizes the photoelastic effect to modulate the phase retardation in a harmonic form [14]. For accurately measuring the ellipsometric parameters with high precision, one has to align the strain axis of PEM to the incident plane and calibrate its modulation amplitude. Since the incident plane has been well aligned in the PSA ellipsometry, one can easily align the strain axis to the incident plane by null and then determine its axis directly through the measurements of two DC

intensities when the azimuths of the analyzer are separated by 45°. Regarding the modulation amplitude of PEM, although one can use the waveform of its half-wave in an oscilloscope to calibrate the modulation amplitude, it is usually very hard to visualize the flat shape of the waveform while its modulation amplitude is at half-wave. Recently, there is great progress in the data acquisition (DAQ) system with multi-functions. In this chapter, we perform the two options of the DAQ system for aligning the strain axis and calibrating the modulation amplitude of PEM in the ellipsometry: (1) lock-in amplifiers and (2) digitized oscilloscope. Since the digitized waveform can be stored for analyzing, the system errors of PEM controller can be inspected.

4.1. Alignment of the strain axis of PEM

The basic setup of the PEM ellipsometer is shown in **Figure 16**. If the azimuth angle of the initial linear polarized light is set at 45°, and the strain axis of PEM deviates from the incident plane by θ, the measured intensity can be simplified as

$$I(A) = I_0 \left[L \sin^2 A + M \cos^2 A \ \tan^2 \Psi + N \sin A \ \cos A \right] \tag{19}$$

where

$$L = 0.5[1 + \cos\Delta_P + (1 - \cos\Delta_P)(1 - \sin\Delta_P)] \tag{20}$$

$$M = 0.5[1 + \cos\Delta_P + (1 - \cos\Delta_P)(1 + \sin 4\theta)] \tag{21}$$

$$N = 0.5[1 + \cos\Delta_P - (1 - \cos\Delta_P)\cos 4\theta] \tan\Psi \ \cos\Delta - \sin\Delta_P \ \cos 2\theta \ \tan\Psi \ \sin\Delta \tag{22}$$

The modulation amplitude Δ_p of PEM is modulated as $\delta_0\cos(\omega t)$. By setting the azimuth angle of analyzer at 0°, the measured intensity can be expressed as
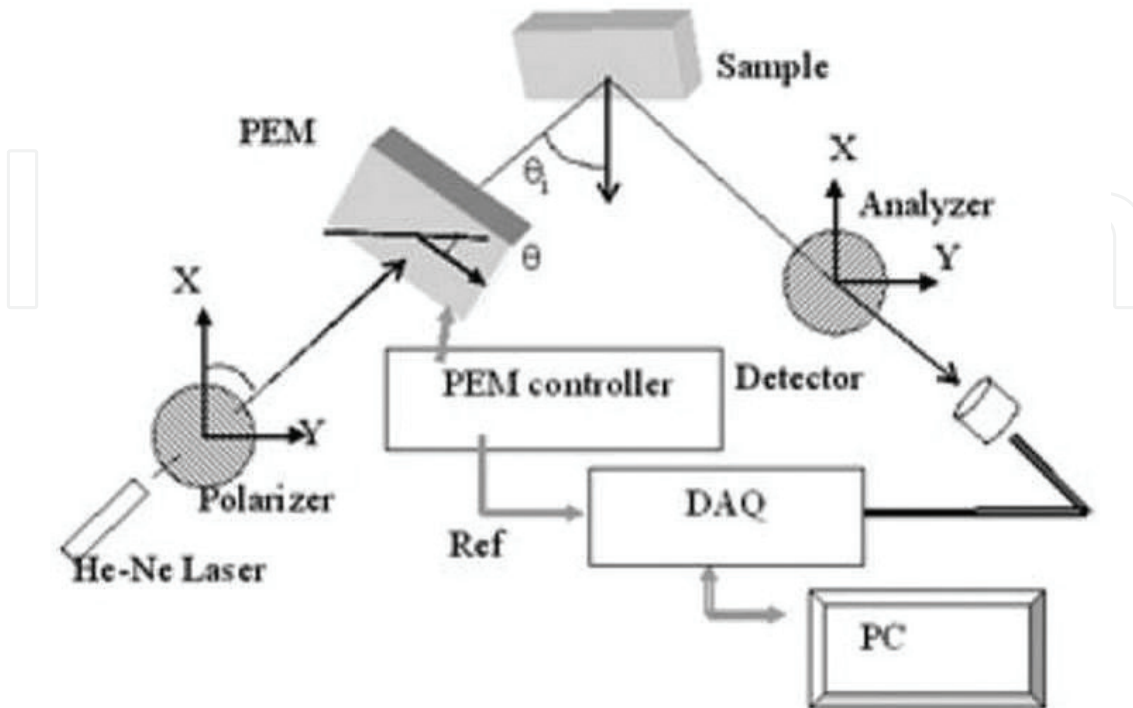

Figure 16. Schematic setup of PEM ellipsometer.

$$I(0°) = 0.5I_0 \tan^2\Psi \ [2 + (1 - \cos\Delta_P)\sin 4\theta] \tag{23}$$

then the intensity can be Fourier expanded by its harmonic function

$$\cos\Delta_P = J_0(\delta_0) - 2J_2(\delta_2)\cos 2\omega t \ldots \tag{24}$$

By taking the zero-order Bessel function $J(\delta_0)$ at its zero point, that is, $\delta_0 = 0.383\lambda$, we can simplify the DC component of its intensity as

$$I_{dc}(0°) = 0.5I_0 \tan^2\Psi \ [2 + \sin 4\theta] \tag{25}$$

From this equation, the strain axis of PEM deviates from zero by $\theta°$, which can be measured by the DC component of the intensity. Taking two I_{dc} at θ_0 and $\theta_0 + 45°$, one can obtain θ_0 through the following relation:

$$\sin 4\theta_0 = 2\frac{I_{dc}(0°)_{\theta=\theta_0} - I_{dc}(0°)_{\theta=\theta_0+45°}}{I_{dc}(0°)_{\theta=\theta_0} + I_{dc}(0°)_{\theta=\theta_0+45°}} \tag{26}$$

A typical result after rough alignment is shown in **Figure 17**. According to the intensity ratio of Eq. (26), one can easily prove that the deviation of azimuth $\delta\theta_o$ resulting from those intensity fluctuations is
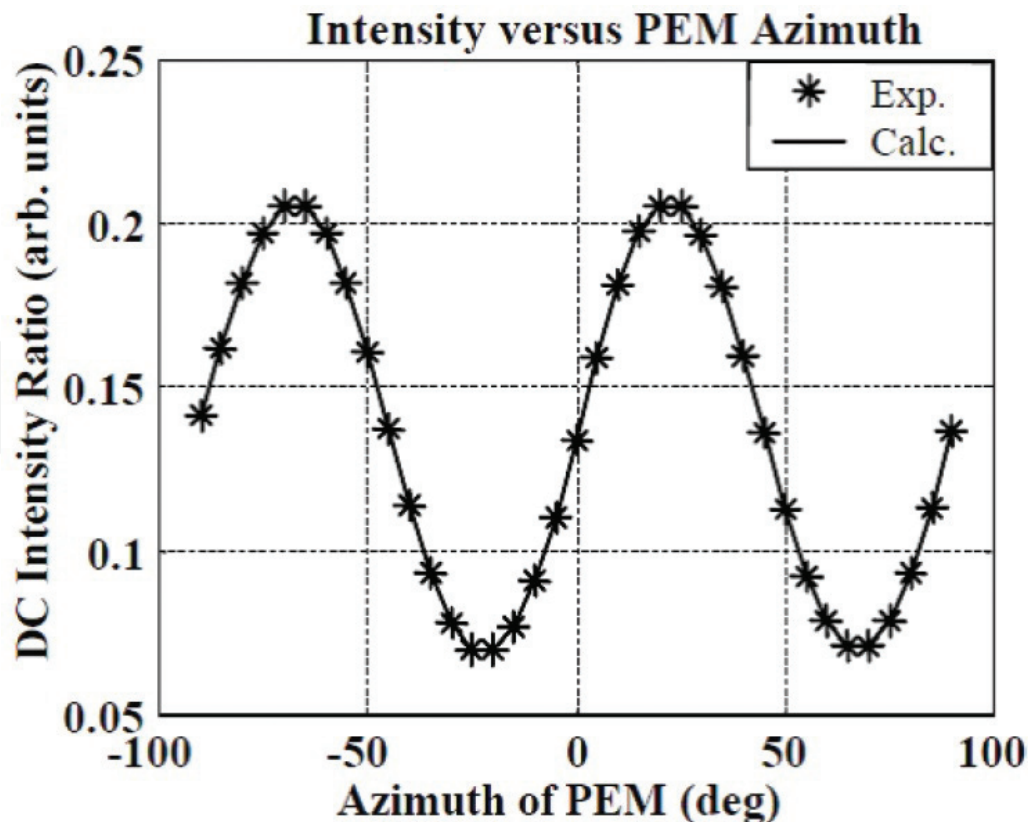

Figure 17. DC intensity distribution of the PEM ellipsometer. The azimuth angle of A is at 0° versus the azimuthal angle of the strain axis of PEM. *The experimental data and the solid line show the intensity distribution when the strain axis of PEM is at 0.2764±0.0003°.

$$\delta\theta_0 = \frac{\tan 4\theta_0}{4\tan^2\Psi}\frac{\delta I}{I} \tag{27}$$

The intensity fluctuation can be large at $\theta_0 = 22.5°$, which is far away from the roughly aligned value. By readjusting the θ_0 to zero, one can obtain a well-aligned PEM ellipsometry.

4.2. Calibration of the modulation amplitude of PEM

According to the last section, the strain axis of PEM can be well aligned to the incident plane, θ is zero, and the azimuth of polarizer is at 45°, Eq. (19), can be simplified as

$$I(A) = 0.5I_0\left[\sin^2 A + \tan^2\Psi\ \cos^2 A - \tan\Psi\ \sin 2A\ (\cos\Delta\ \cos\Delta_P + \sin\Delta\ \sin\Delta_P)\right] \tag{28}$$

Since the Fourier expansions of the harmonic functions are

$$\sin\Delta_P = 2J_1(\delta_0)\sin\omega t + 2J_3(\delta_0)\sin 3\omega t + \ldots \tag{29}$$

$$\cos\Delta_P = 2J_0(\delta_0) + 2J_2(\delta_0)\sin 2\omega t + 2J_4(\delta_0)\cos 4\omega t + \ldots \tag{30}$$

One can prove the following relation for the measurement of Ψ and Δ:

$$\sin 2\Psi = \frac{\sqrt{\left(\frac{I_{1f}(45°)}{J_1(\delta_0)}\right)^2 + \left(\frac{I_{2f}(45°)}{J_2(\delta_0)}\right)^2}}{I_{dc}(45°) + I_{dc}(-45°)} \tag{31}$$

$$\tan\Delta = \frac{I_{1f}(45°)J_2(\delta_0)}{I_{2f}(45°)J_1(\delta_0)} \tag{32}$$

It is very interesting to notice that the even/odd harmonics are related by the similar physical parameters except the orders of its Bessel function. So,

$$\frac{I_{1f}}{I_{3f}} = \frac{J_1(\delta_0)}{J_3(\delta_0)} \tag{33}$$

$$\frac{I_{2f}}{I_{4f}} = \frac{J_2(\delta_0)}{J_4(\delta_0)} \tag{34}$$

The modulation amplitude δ_0 can be measured by the intensity ratio of even/odd harmonics. In the operation menu of PEM [15], the value δ_0 can be calibrated by the oscilloscope waveform of a half-wave, that is, $\delta_0 = 0.5$, such as shown in **Figure 18**. However, when one is constructing a new element in a system, some defects are expected. Since one can measure the modulation amplitude by the even/odd intensity ratios, one can calibrate the modulation amplitude and compare it with the digitized oscilloscope waveform obtained from DAQ system, such as shown in **Figure 19**. The system errors, azimuth angle, and modulation amplitude can be corrected after the alignment and calibration in order to establish an accurate PEM ellipsometer.
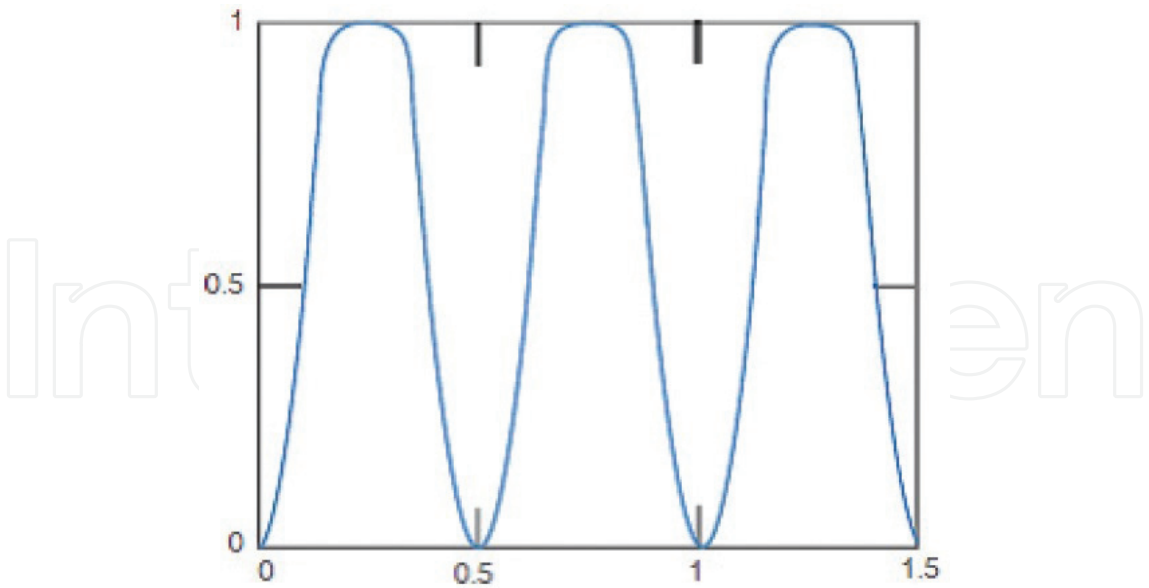
Figure 18. The oscilloscope waveforms when the modulation amplitude of PEM is a half-wave [15].
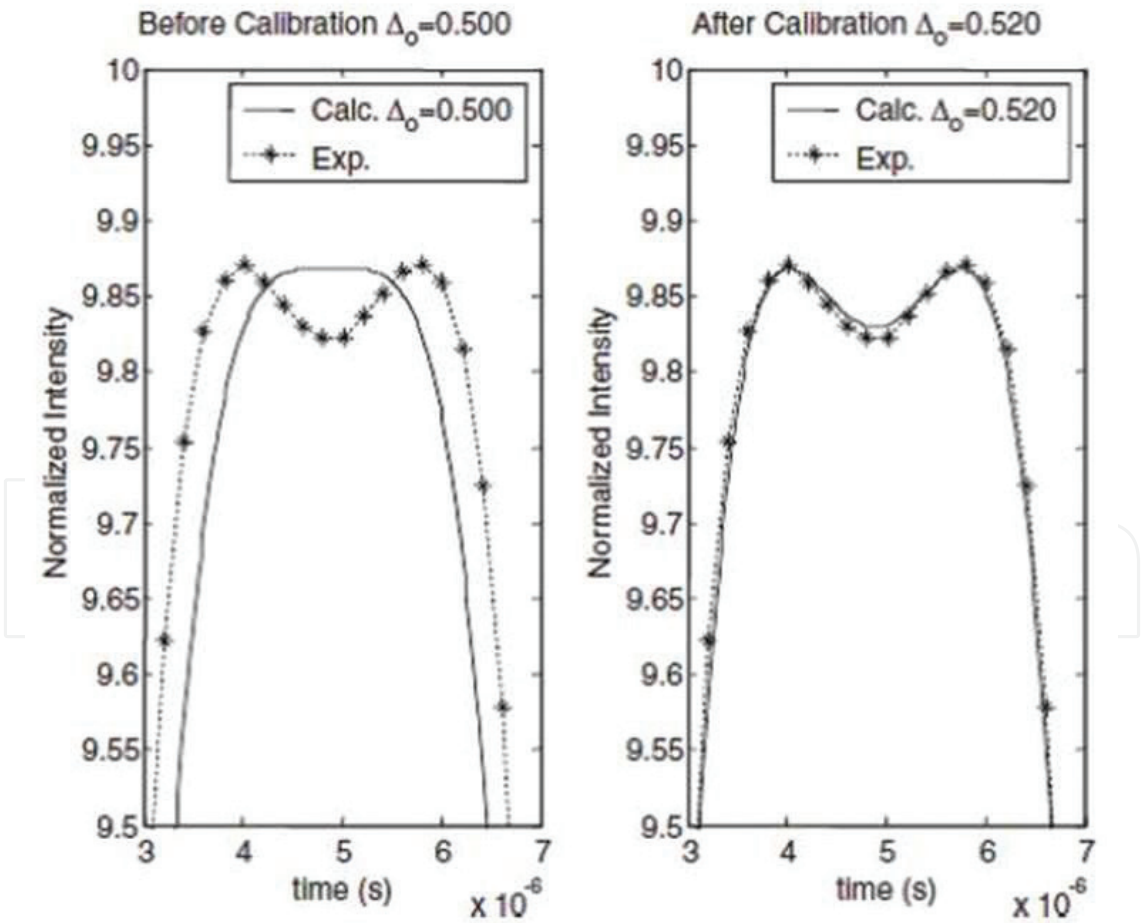

Figure 19. Recorded digitized oscilloscope waveform when the modulation amplitude of PEM has been claimed as half-wave: left—before calibration and right—after calibration.

4.3. Applications

For monitoring the physical processes, plasma etching [16], deposition [17], thermal heating [18], and photo-induced [19], one has to establish the in situ alignment technique for PEM ellipsometry. A DAQ card is an analog-to-digital converter. In the PEM ellipsometry, the multi-function DAQ (typical PCI-6111) can be used as two lock-in amplifiers for real-time measurement (10 sets/s), and post-flight analysis, that is, analyze the reflected waveform of the digital oscilloscope specification of the DAQ system, so the data rate can reach 25,000 sets/s. With the help of a stroboscope to modulate the light source, one can lock the wave at four specific phases to measure the ellipsometric parameters of the testing sample. By using CCD as the detector, an imaging ellipsometry can also be established in the PEM ellipsometry. The followings are examples for the applications of PEM ellipsometry.

4.3.1. Plasma etching

For monitoring the etching process, a plasma-etching chamber can install a PEM ellipsometer to monitor the etching process, such as the schematic setup shown in **Figure 20**. A thick wafer is used to extract the etched thickness under etching, which can be monitored by the PEM ellipsometry to avoid over-etch. After calibrating the modulation amplitude, one can etch the film to the targeted thickness by monitoring the behavior of Ψ and Δ with the theoretical predication in real time. For example, we target a thick SiO_2 on polysilicon started from around 500 nm to be etched to 30 nm. The measured value with the theoretical value, such as
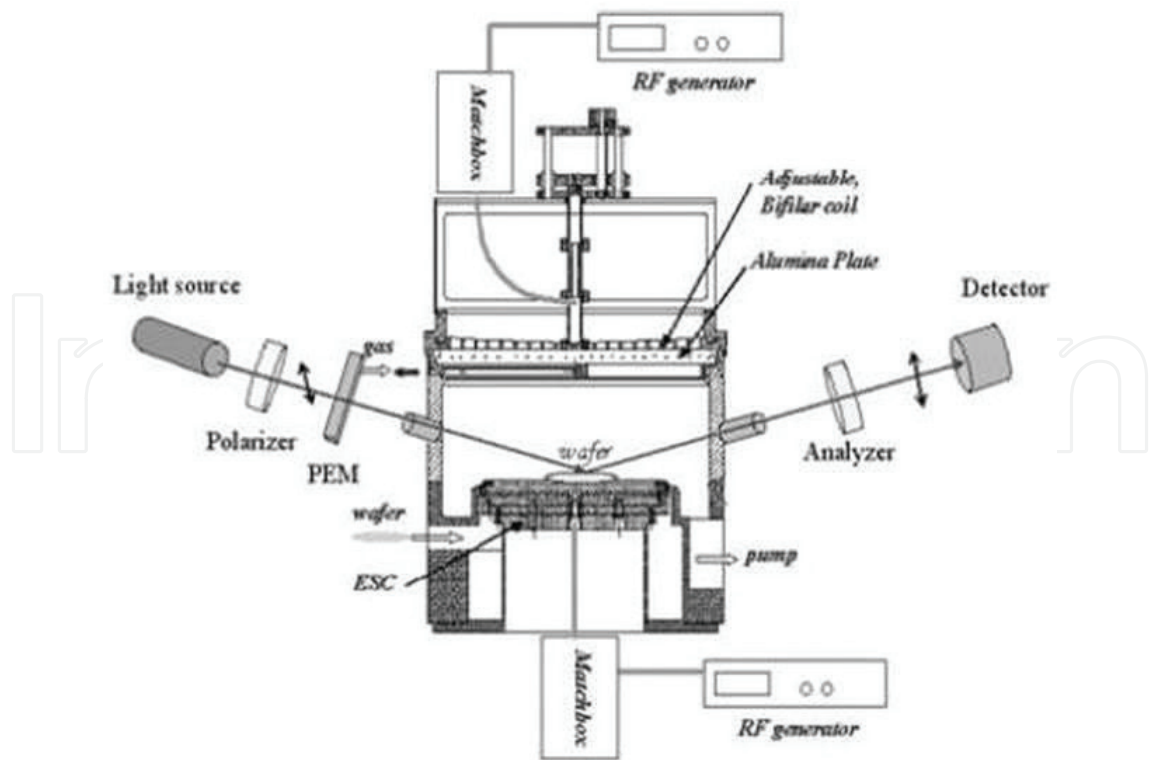

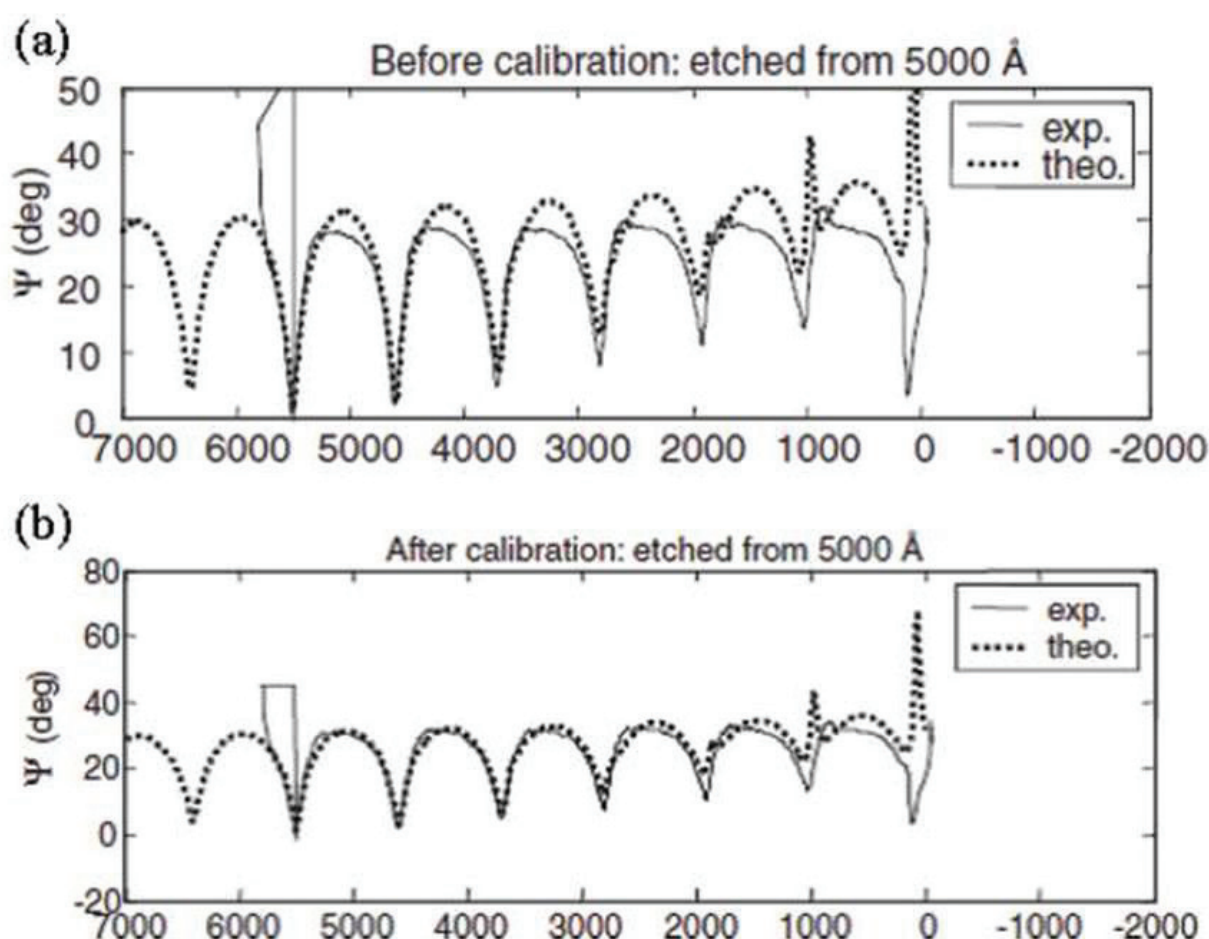**Figure 20.** Schematic setup of the IPC etcher.

Figure 21. Distributions of Ψ for film etched from 500-nm thickness of SiO_2 on silicon substrate (a) before calibration and (b) after calibration: (dotted line) theoretical value; (solid line) measured value $\times$ fc [16].

in **Figure 21a**, the histogram of Ψ before correction, and **Figure 21b**, the histogram of Ψ after correction (fc, the correction factor from the measurement of modulation amplitude), can be compared. In the corrected curve, we observed the behavior of etching: the sharp rising of Ψ in the end cycle, around 70 nm. In the end, we can control the etching process: the etching stopped at the thickness of the film to be close to 30 nm within 0.2 nm, such as shown in **Figure 22**.

4.3.2. Thermal heating

The perovskite materials are attractive because they exhibit extremely high piezoelectric coefficients and a wide region of controlled dielectric constants when the compositions are near the morphotropic phase boundary (MPB) [20]. In previous studies, doping Ru into complex oxides can enhance the photorefractive effect in the red and near-infrared spectral regions [21]. In addition, using Ru as a dopant in various inorganic crystals can considerably improve their response time and photoconductivity [22]. Therefore, Ru-doped perovskites can be considered as practical material for optical memories. In the process of storage, the temperature of the surroundings can fluctuate due to laser irradiation, heat dissipation, and so on. However, for
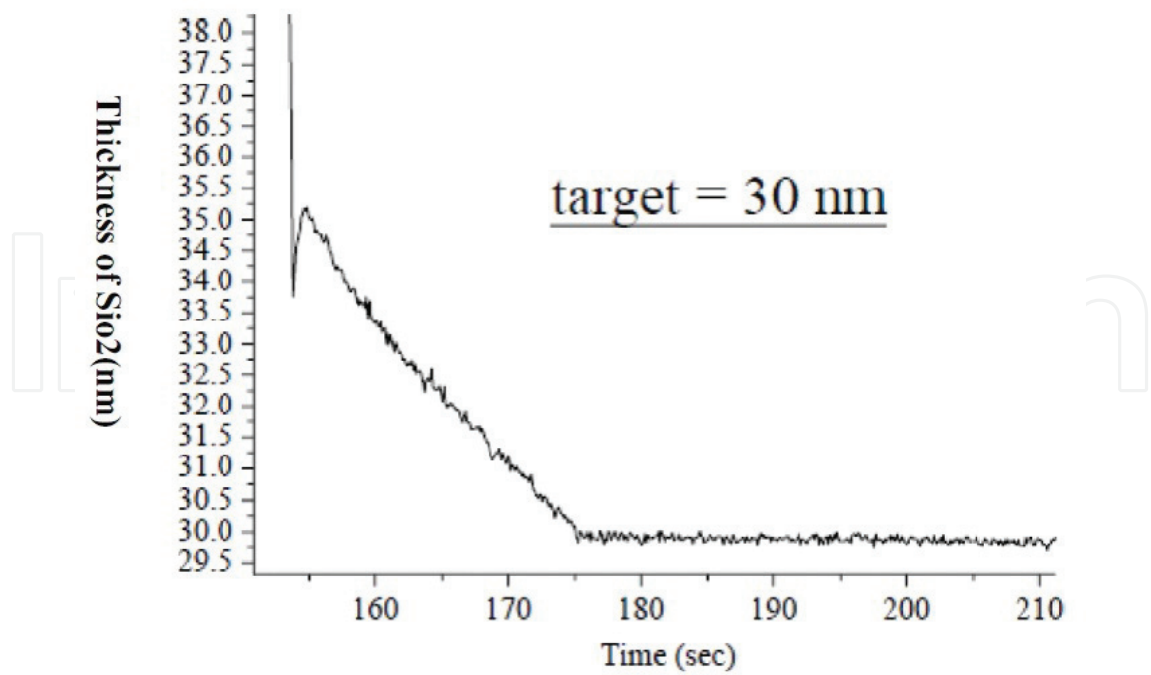
Figure 22. The histogram of an etching of SiO₂/Si, the target of the process was 30 nm.

optical storage, the refractive index of the perovskite material must be stable under the working temperature. It will be interesting to measure their refractive indices during heating in order to understand what would be the most favorable working temperature for optical storage. One can setup the PEM ellipsometry as shown in **Figure 23** to monitor the refractive index of perovskite material under heating. In the thermally isolated chamber, the samples can be heated from room temperature to 200°C by the thermoelectric cooler (TE cooler), which operates based on the Peltier effect, so it can be used as heater when the electric current is
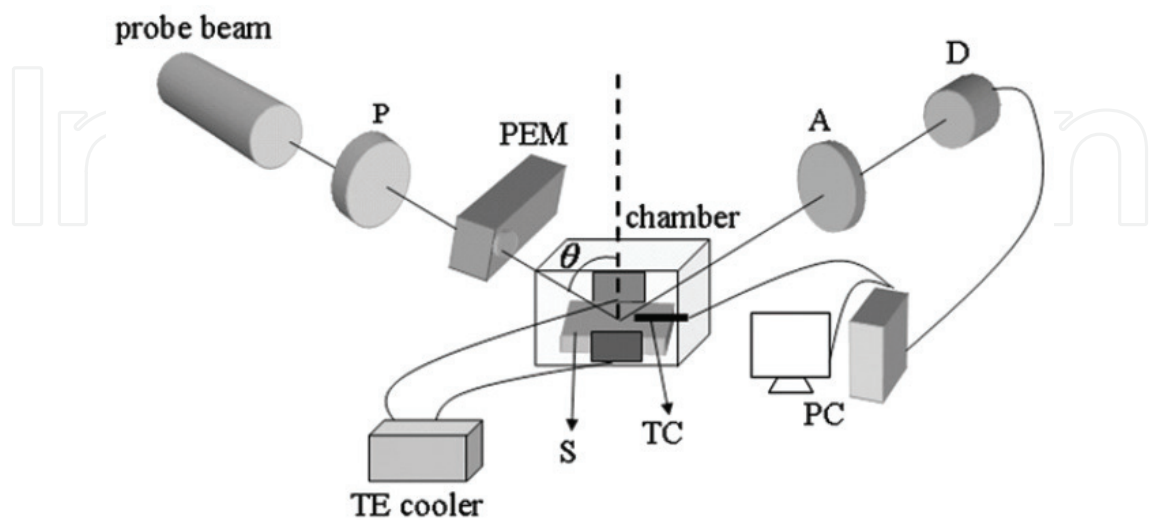

Figure 23. Schematic setup of the PEM ellipsometer for measuring the variation in the refractive index during the heating process: probe beam: HeNe laser (632.8 nm); P: polarizer; PEM: photoelastic modulator; S: sample; θ: incident angle.
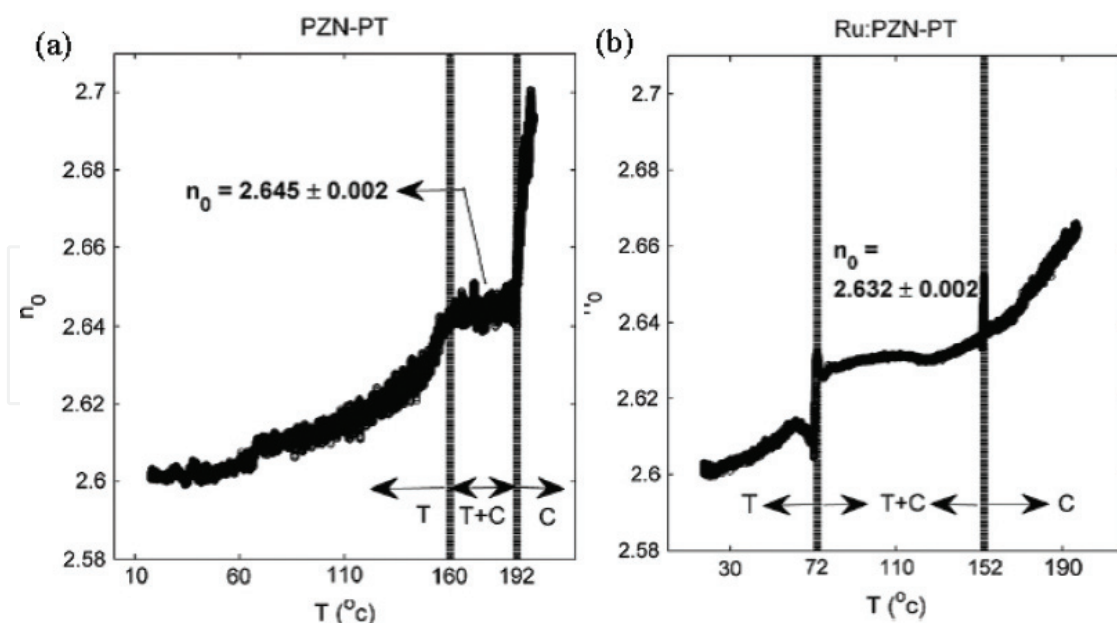
Figure 24. Refractive indices of (a) pure 0.9PZN-0.1PT and (b) Ru-doped 0.9PZN-0.1PT against temperature during heating: T: tetragonal; C: cubic.

inversely applied. The TE cooler is small but highly reliable. The sample can be sandwiched between two TE coolers to maintain uniformity of temperature of the sample. A k-type thermocouple was attached to the surface of the sample to monitor the temperature. The voltage produced by the thermocouple can be acquired by one of the channels of the same data acquisition system. The voltage is then converted to the required temperature scale according to the NIST ITS-90 Thermocouple Database. In this way, both the temperature and the ellipsometric parameters can be simultaneously monitored. According to the study by Chuang et al. [18], the ellipsometric parameters of pure and Ru-doped 0.9PZN–0.1PT were measured by PEM ellipsometry with a sampling rate of 10 sets/s. The refractive indices were converted from the measured Ψ and Δ, such as shown in **Figures 24a** and **b**. From the results of the experiment, one can conclude that when Ru is used as a dopant in 0.9PZN–0.1PT, the Curie region is broadened and shifted closer to room temperature. Therefore, the PEM ellipsometry can be used to analyze the behavior of material under heating.

4.3.3. Photo-induced effect

Holographic data storage has been considered to be a promising data storage technology because it provides high storage density and fast readout rate. One of the fundamental issues for this technique to be successful is the availability of thick recording materials. Recently, research involving organic photopolymers has become of interest because of the flexibility for fabrication. Photopolymers exhibit a photorefractive effect, and the photo-induced changes in the refractive index can be used to record the holographic interference pattern in order to form phase grating. Based on this idea, many new photopolymers have been synthesized and studied. The photo-induced refractive index variation and photo-induced birefringence are two of the most often used mechanisms for producing the necessary changes in refractive
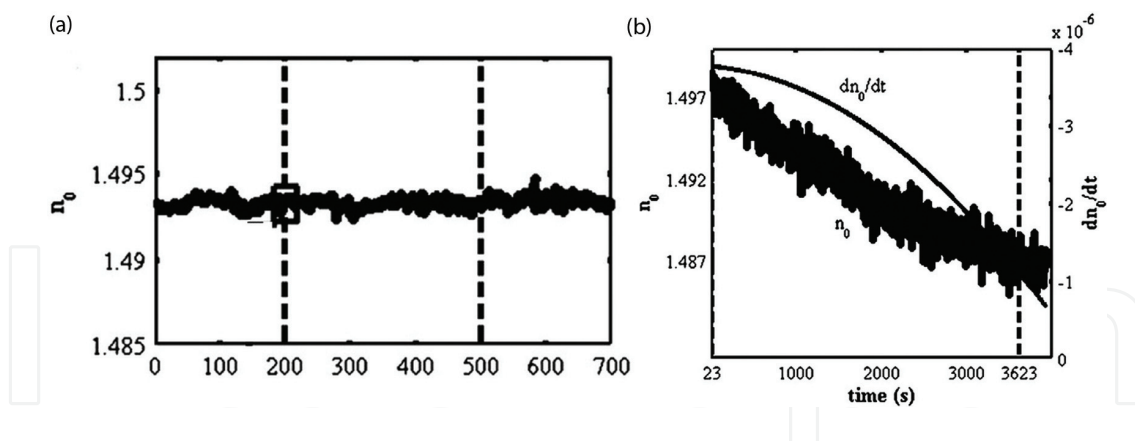
Figure 25. Histogram of measured refractive index during heating: (a) pure PMMA: the 488-nm laser was turned on at the 200th second and then turned off at the 500th second. The average refractive index is 1.493±0.003; (b) PQ-doped PMMA: the 488-nm laser was turned on at the 23rd second and turned off at the 3623rd second; the refractive changes from 1.497 to 1.487. It is exposed to 488 nm (Ar/Kr tunable laser) with total exposure energy density of 68.4 J/cm^2.

indices for holographic recording. Thus, various methods have been proposed for investigating these two effects in different photopolymers for further improving the properties of the recording materials. The refractive indices of the photopolymers have been measured by an Abbe refractometer and a prism coupler, but the variation of the refractive index is commonly extracted from the diffraction formula by measuring the diffraction efficiency of a recorded grating [23]. Since the PEM ellipsometry can measure the refractive index during exposure, one can compare the photorefractive effect of photopolymers under irradiation. The PEM ellipsometry was used to measure the pure and doped PMMA, such as shown in **Figures 25a** and **b**. From these two measurements, one can conclude that the holographic recording in PQ-doped PMMA was mainly due to the change in the refractive index. The change in the refractive index is produced by molecular structure changes of the PQ molecules. This in situ/real time can observe the structure change under irradiation.

4.3.4. Post-flight analysis

Since most data acquisition systems are multi-function systems, if the PEM ellipsometry employs its function of lock-in amplifier to measure dc, 1f, and 2f signals for deducing the ellipsometric parameters, one can only obtain a data rate of 10 sets/s. In Section 4.2, the DAQ system has been used as digital oscilloscope for calibrating the modulation amplitude of PEM. The waveform obtained from the digital oscilloscope can be stored for post-flight analysis. The ellipsometric parameters can be obtained by fast Fourier transform of the stored waveform. In this case, the PEM ellipsometry can reach the speed limit of PEM, since Hinds PEM90 operated at an oscillating frequency around 50 kHz, so its data rate can reach 25,000 sets/s, for example, if one wishes to measure the response time of twisted nematic liquid crystals. It is known that the response time of twisted nematic liquid crystals (TN-LC) is in the millisecond regime, the transmitted PEM-DAQ ellipsometry can be used to analyze the variation of its ellipsometric parameters under a square wave. **Figure 26** shows the histogram of the ellipsometric parameters of a TN-LC cell applying a 5-Hz square wave with a step voltage of 5 V. From the graph, one can measure the rising time and fall time of the TN-LC, which are 7.5 and 19 ms, respectively.
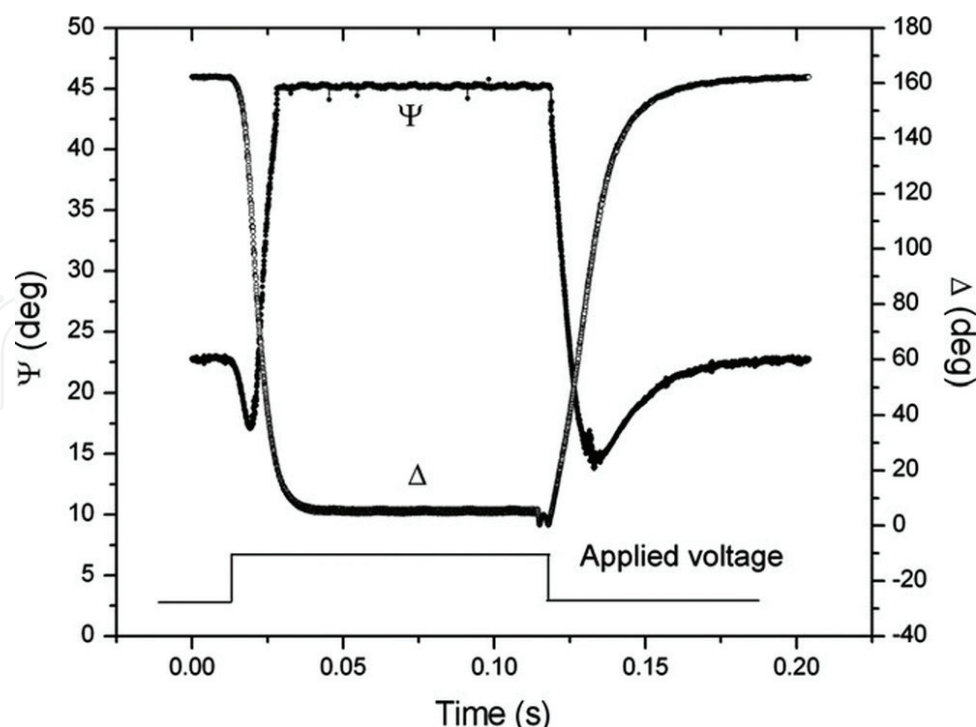
Figure 26. Histograms of measured ellipsometric parameters for the twisted nematic liquid crystal cell (transmission ellipsometry, λ = 632.8 nm). A square wave of 5 Hz and strength 5 V was applied.

The generalized ellipsometry (GE) has been developed to measure the refractive indices of anisotropic crystals [24]. In GE, at least three polarization states have to be used for extracting the physical parameters of anisotropic crystals. Using a fixed polarizer and PEM, one can generate various polarization states (200/cycle, Hinds90) because of the harmonic oscillation property of PEM. Two modulators of generalized ellipsometry [25] have been developed to measure the anisotropic medium. Due to the development of inverse problem in optics, Chuang et al. [26] implemented the program of Hodgkinson (BTF tool box) to simulate the reflected intensity profile. This profile can be analyzed and compared with the digitized waveform obtained from DAQ system of PEM ellipsometer. In his study, he found a distinguished characteristic in the reflected waveform for different complex refractive indices. Instead of using the Fourier transform on the waveform, he analyzed the reflected/transmitted waveform to extract the physical parameters. In the same reference, he proved that two incident angles are required to extract the complex refractive indices and the orientation of its optical axis of the anisotropic crystal. First, he concentrated his analysis on the reflected waveform at the incident angle of 70°. According to the Fresnel reflection coefficient of a uniaxial crystal, one can graph the normalized reflected intensity waveform as **Figure 27a**. The asymmetric distribution provides the information of absorbing or nonadsorbing materials. Assume k_{ave} = 0.5(k_e+k_o) and Δk = k_e−k_o are the averaged and difference between the extinction of ordinary and extraordinary coefficients, respectively, and n_{ave} = 0.5(n_e+n_o) and Δn = n_e−n_o are the averaged and difference between ordinary and extraordinary refractive indices, respectively. Using **Figures 27b** and **c**, one can conclude that the value of averaged extinction coefficient and difference can be estimated from the height (H) of the dip by the parametric
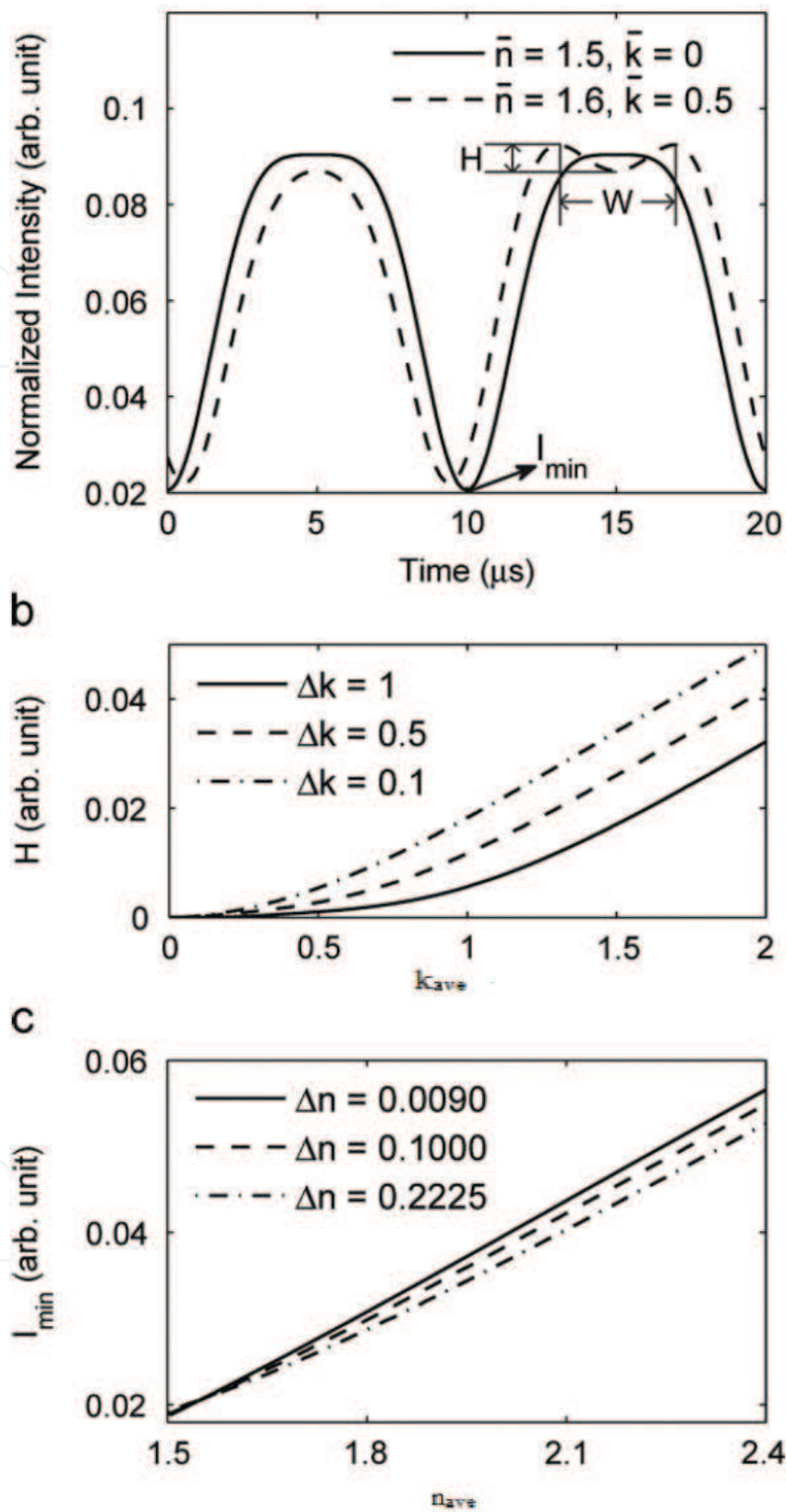
Figure 27. Estimation for complex refractive index (θ_i=70°): (a) the normalized reflected intensity profile; (b) the parametric equations of the dip depth (H) versus the averaged extinction coefficient (k_{ave}); and (c) the parametric equations of the minimum intensity (I_{min}) versus the averaged refractive indices (n_{ave}).

$k_{ave} = 0.5(k_e + k_o)$	$H_{70} = p_0 + p_1 k_{ave} + p_2 k_{ave}^2$
$\Delta k = k_e - k_o$	$p_0 = -0.002 + 0.003\Delta k$
	$p_1 = -0.015 + 0.021\Delta k$
	$p_2 = 0.006 + 0.005\Delta k$

Table 4. The parametric equations of dip height H for estimating the extinction coefficients obtained by simulated reflected waveform when θ_i at 70°.

$n_{ave} = 0.5(n_e + n_o)$	$I_{70min} = q_0 + q_1 n_{ave}$
$\Delta n = n_e - n_o$	$q_0 = -0.046 + 0.031\Delta n$
	$q_1 = 0.043 + 0.022\Delta n$

Table 5. The parametric equations of I_{min} for estimating the refractive coefficient obtained by simulated reflected waveform when θ_i at 70°.

equations (**Table 4**). The averaged refractive index can be estimated by the minimum intensity I_{min} of the waveform, which is linearly related to the average refractive index (**Table 5**). It is known that the genetic algorithm is the mechanism of nature evolution and is considered as the optimal solution in the complex multidimensional search spaces. The parametric equations really can narrow down the searching region in genetic algorithm. Since the genetic algorithm [27] has been applied in ellipsometry, one can simulate the waveform and find the characteristic property to narrow down the searching region, then to search the complex refractive indices and the orientation of optical axis. Using two optimized incident angles, Chuang et al. [26] extracted the n_o and n_e of quartz crystal to be 1.543 and 1.552, respectively. In addition, the orientation of its optical axes was also measured from the same
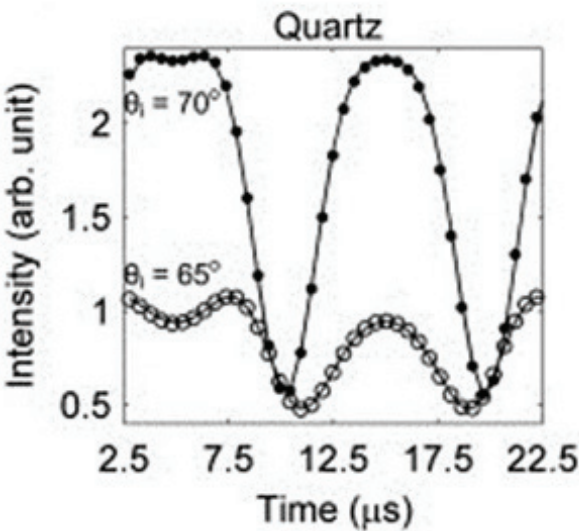

Figure 28. Measured reflected intensity profiles of quartz at incident angles of 65° (o) and 70° (●). All these measured values are compared with the calculated values (-). Only 1/5 data points in each cycle are displayed.

waveform. **Figure 28** shows the comparison between simulated waveform by using the extracted physical parameters (refractive indexes, orientation of optical axis) and measured values. This work presents the powerfulness of the post-flight analysis technique; one only has to use one cycle (20 μs of Hinds PEM 90) of the reflected intensity signals to extract all the optical parameters.

5. Future prospects

The three-intensity measurements technique in PSA ellipsometry can be easily constructed into the imaging ellipsometry. In this system, the rotation of polarizer and analyzer not only slows down the measuring speed but also causes the incident beam to deviate from its setting. This is the reason for establishing the PEM ellipsometry. However, the modulation frequency of PEM is very high (most PEM operates in 50 kHz), and one must use fast response detector for PEM ellipsometry. The operation of CCD camera is a time-consuming process in comparing with the modulation frequency of PEM. The PEM imaging ellipsometry can only be established by employing the modulated laser diode as pulse for strobe illumination [28] at four specific phases. In this technique, one has to calibrate the initial phase for synchronizing the four specific phases to perform ellipsometric measurements. Again, with the help of symbolic computer program, Mathematica, Tsai [29] de-associated the initial phase by extra strobe measurement. This PEM stroboscopic imaging ellipsometry can measure a moving sample dynamically, such as the motion of dropping oil on SiO_2 film. The speed of measurement can be improved by using high-power light source to reduce the exposure time and high-speed DAQ system to match the data transfer of CCD.

For further developing the ellipsometry, one can use the liquid crystal variable retarder to replace PEM. It is interesting to notice [30] a three-intensity measurements technique in ellipsometry by varying the phase retardation of liquid crystal instead of varying the polarization by rotating any part of the system. In addition to a liquid crystal variable retarder, a quarter wave plate has been introduced to form an ellipsometer without any mechanical motion. The in situ calibration of the liquid crystal variable retarder has to be performed. Just like the three-intensity measurement in PSA ellipsometry, one can install a liquid crystal variable retarder by varying three phases to form an imaging ellipsometry. Polarizer and quarter wave plate can be formed as polarization generator, liquid crystal variable retarder and analyzer can be packed as polarization analyzer. Since all these components are light-weight with low cost, one can construct a compact and portable system for imaging ellipsometric measurements. The only disadvantage of liquid crystal variable retarder is its stability in temperature. For accurate measurement, one has to use a temperature controller. We await the improvement of the liquid crystal variable retarder for the establishment.

Acknowledgements

Author details

Yu-Faye Chao

Address all correspondence to: yfchao@mail.nctu.edu.tw

Department of Photonics, National Chiao Tung University, Taiwan, ROC

References

[1] Azzam RMA, Bashara NM. Ellipsometry and Polarized Light. Paperback. North Holland: Elsevier Science Publishers B.V.; 1987

[2] Collins RW. Automatic rotating element ellipsometers: Calibration, operation, and real-time applications. Review of Scientific Instruments. 1990;**61**:2029-2062. DOI: 10.1063/1.1141417

[3] Chao YF, Wei CS, Lee WC, Lin SC, Chao TS. Ellipsometric measurements and its alignment: Using the intensity ratio technique. Japanese Journal of Applied Physics. 1995;**34**:5016-5019. DOI: 10.1143/JJAP.34.5016

[4] Chao YF, Lee WC, Hung CS, Lin JJ. A three-intensity technique for polarizer-sample-analyser photometric ellipsometry and polarimetry. Journal of Physics D: Applied Physics. 1998;**31**:1968-1974. DOI: 10.1088/0022-3727/31/16/005

[5] Steel MR. Method for azimuthal alignment in ellipsometry. Applied Optics. 1971;**10**:2370-2371

[6] Wang MW, Chao YF. Azimuth alignment in photoelastic modulation ellipsometry at a fixed incident angle. Japanese Journal of Applied Physics. 2002;**41**:3981-3986. DOI: 10.1143/JJAP.41.3981

[7] Chao YF, Lee KY, Lin YD. Analytical solutions of the azimuthal deviation of a polarizer and an analyzer by polarizer-sample-analyzer ellipsometry. Applied Optics. 2006;**45**: 3935-3939. DOI: 10.1364/ao.45.003935

[8] Chao YF, Wang MW, Ko ZC. An error evaluation technique for the angle of incidence in a rotating element ellipsometer using a quartz crystal. Journal of Physics D: Applied Physics. 1999;**32**:2246-2249. DOI: 10.1088/0022-3727/32/17/315

[9] Tomlinson WJ. Application of GRIN-rod lenses in optical fiber communication systems. Applied Optics. 1980;**19**:1127-1138. DOI: 10.1364/AO.19.001127

[10] Garratt J, Mills M. Measurement of the roughness of supersmooth surfaces using a stylus instrument. Nanotechnology. 1996;**7**:13-20. DOI: 10.1088/0957-4484/7/1/002

[11] D'Acquisto L, Fratini L, Siddiolo AM. A modified moiré technique for three-dimensional surface topography. Measurement Science and Technology. 2002;**13**:613-622. DOI: 10.1088/0957-0233/13/4/326

[12] Han CY, Lee ZY, Chao YF. Determining thickness of films on a curved substrate by use of ellipsometric measurements. Applied Optics. 2009;**48**:3139-3143. DOI: 10.1364/AO.48.003140

[13] Han CY, Du CY, Chen YR, Chao YF. Developing a phase and intensity measurement technique with multiple incident angles under surface plasmon resonance condition. Proceedings of SPIE. September 2013;**8905**:89052N:1-7. DOI: 10.1117/12.2035029

[14] Jasperson SN, Schnatterly SE. An improved method for high reflectivity ellipsometry based on a new polarization modulation technique. Review of Scientific Instruments. 1969;**40**:761-767. DOI: 10.1063/1.1684062

[15] Oakberg T, Wang B. Light intensity modulation using a PEM. Technology for Polarization Measurement. 2000:1-3 http://www.hindsinstruments.com/wp-content/uploads/Light-Intensity-Modulation.pdf

[16] Wang MW, Chao YF, Leou KC, Tsai FH, Lin TL, Chen SS, et al. Calibrations of phase modulation amplitude of photoelastic modulator. Japanese Journal of Applied Physics. 2004;**43**:827-832. DOI: 10.1143/JJAP.43.827

[17] Collins RW. In situ ellipsometry of thin-film deposition: Implications for amorphous and microcrystalline Si growth. Journal of Vacuum Science & Technology. B. Microelectronics and Nanometer Structure. 1989;**B7**:1155-1164. DOI: 10.1116/1.584566

[18] Chuang CI, Marinova V, Lin SH, Chao YF. Phase-modulated ellipsometry for probing the temperature-induced phase transition in ruthenium-doped lead zinc niobate-lead titanate single crystal. Thin Solid Films. 2011;**519**:2867-2869. DOI: 10.1016/j.tsf.2010.12.085

[19] Chuang CI, Hsiao YN, Lin SH, Chao YF. Real-time measurement of photo-induced effects in 9,10-phenanthrenequinone-doped poly(methyl methacrylate) photopolymer by phase-modulated ellipsometry. Optical Communication. 2010;**283**:3279-3283. DOI: 10.1016/j.optcom.2010.04.036

[20] Liu W, Ren X. Large piezoelectric effect in Pb-free ceramics. Physical Review Letters. 2009;**103**:257602 1-4. DOI: 10.1103/PhysRevLett.103.257602

[21] Lin CH, Huang CY, Chang JY. Increasing the conductivity of photorefractive $BaTiO_3$ single crystals by doping Ru. Applied Surface Science. 2003;**208–209**:340-344. DOI: 10.1016/S0169-4332(02)01393-4

[22] Rakitina L, Gospodinov M, Briat B. Photorefractive and photochromic properties of Ru doped Sr0:61Ba0:39Nb2O6 crystal. Optical Communication. 2002;**213**:373-378. DOI: 10.1016/S0030-4018(02)02124-7

[23] Robinson TG, DeCorby RG, McMullin JN, Haugen CJ, Kasap SO, Tonchev D. Strong Bragg gratings photoinduced by 633-nm illumination in evaporated As2Se3 thin films. Optics Letters. 2003;**28**:459-461. DOI: 10.1364/OL.28.000459

[24] Azzam RMA, Bashara NM. Application of generalized ellipsometry to anisotropic crystals. Journal of the Optical Society of America. 1974;**64**:128-133. DOI: 10.1364/JOSA.64.000128

[25] Jellison GE, Modine F. Two-modulator generalized ellipsometry: Theory. Applied Optics. 1997;**36**:8190-8198. DOI: 10.1364/AO.42.003765

[26] Chuang CI, Lin SH, Chao YF. Rapid and accurate extraction of optical parameters for uniaxial bulk media by phase modulated ellipsometry. Optics and Lasers in Engineering. 2013;**51**:861-866. DOI: 10.1016/j.optlaseng.2013.02.004

[27] Cormier G, Boudreau R. Genetic algorithm for ellipsometric data inversion of absorbing layers. Journal of the Optical Society of America A: Optics, Image Science and Vision. 2000;**17**:129-134. DOI: 10.1364/JOSAA.17.000129

[28] Han CY, Chao YF. Photoelastic modulated imaging ellipsometry by stroboscopic illumination technique. Reviews in Scientific Instruments. 2006;**77**:1-5. DOI: 10.1063/1.2173027

[29] Tsai HM, Chen CW, Tsai TH, Chao YF. Deassociate the initial temporal phase deviation provided by photoelastic modulator for stroboscopic illumination polarization modulated ellipsometry. Reviews in Scientific Instruments. 2011;**82**:5-10. DOI: 10.1063/1.3568745

[30] Shih W, Hsieh M, Chao YF. A compact in-situ ellipsometer using the liquid crystal variable retarder. Proceedings of SPIE. September 5, 2014;**9200**:1-7. DOI: 10.1117/12.2060567